Mantle convection

Compressible vs. incompressible

C. Thieulot (c.thieulot@uu.nl)

March 2019

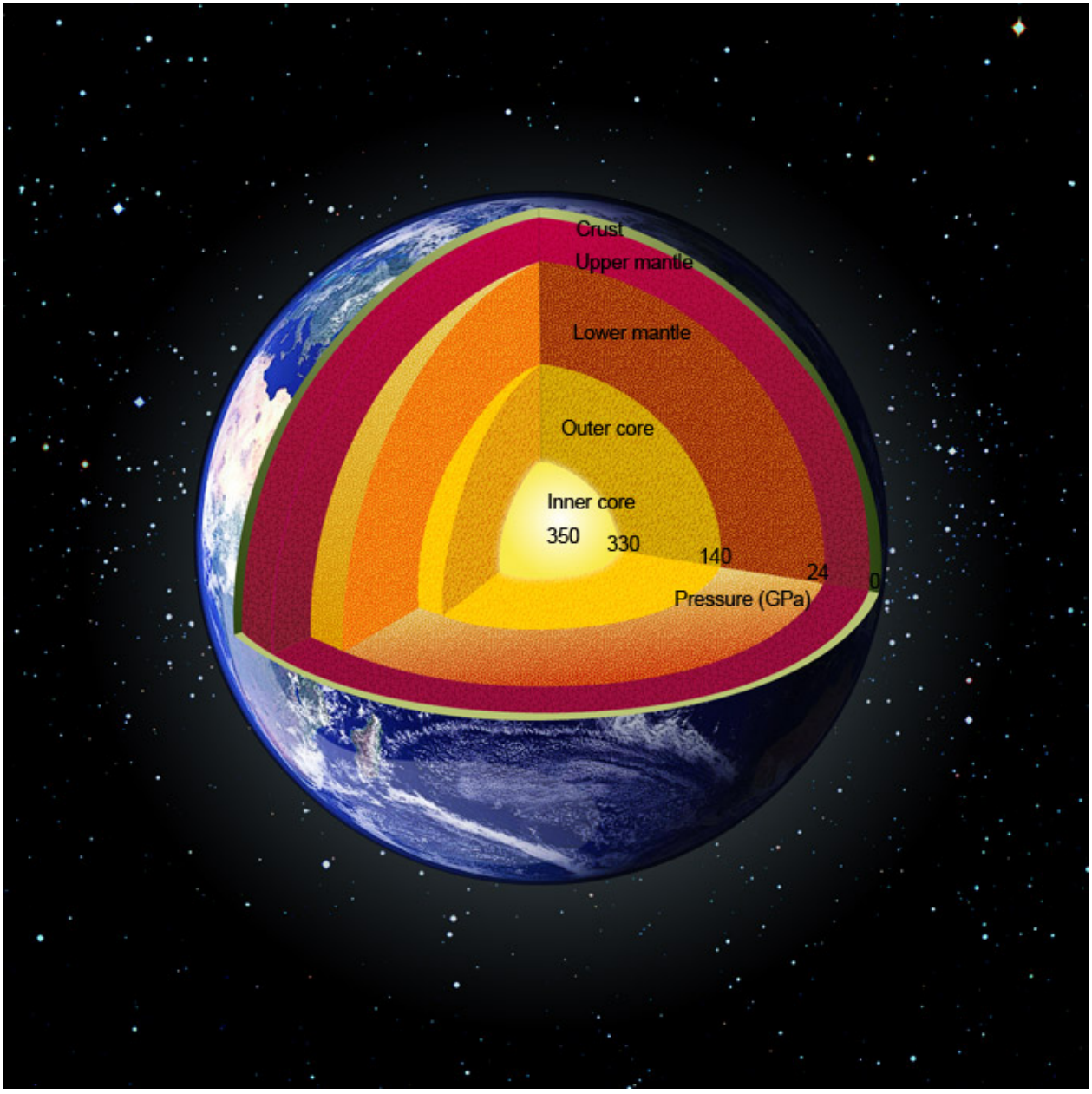
Crust
Upper mantle
Lower mantle
Outer core
Inner core
350
330
140
24
0
Pressure (GPa)

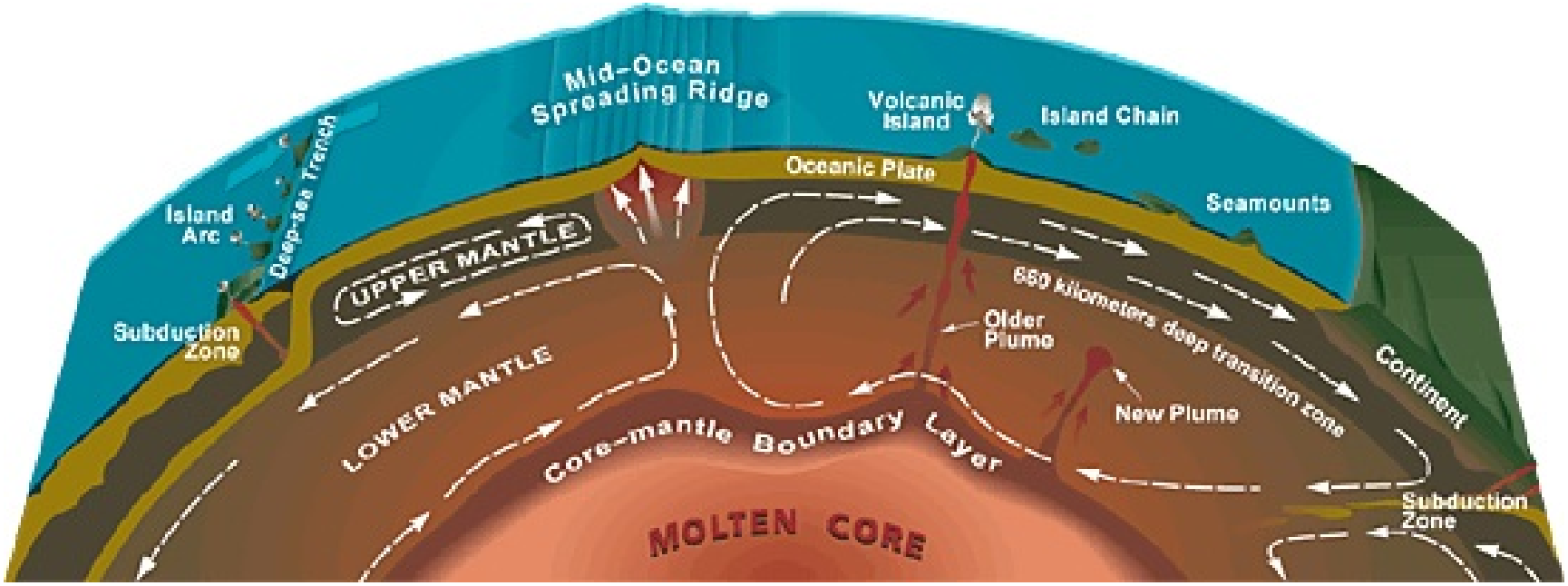
Mid-Ocean
Spreading Ridge
Volcanic
Island
Island Chain
Oceanic Plate
Seamounts
Deep-sea Trench
Island
Arc
UPPER MANTLE
660 kilometers deep transition zone
Older
Plume
Subduction
Zone
LOWER MANTLE
New Plume
Continent
Core-mantle Boundary Layer
Subduction
Zone
MOLTEN CORE

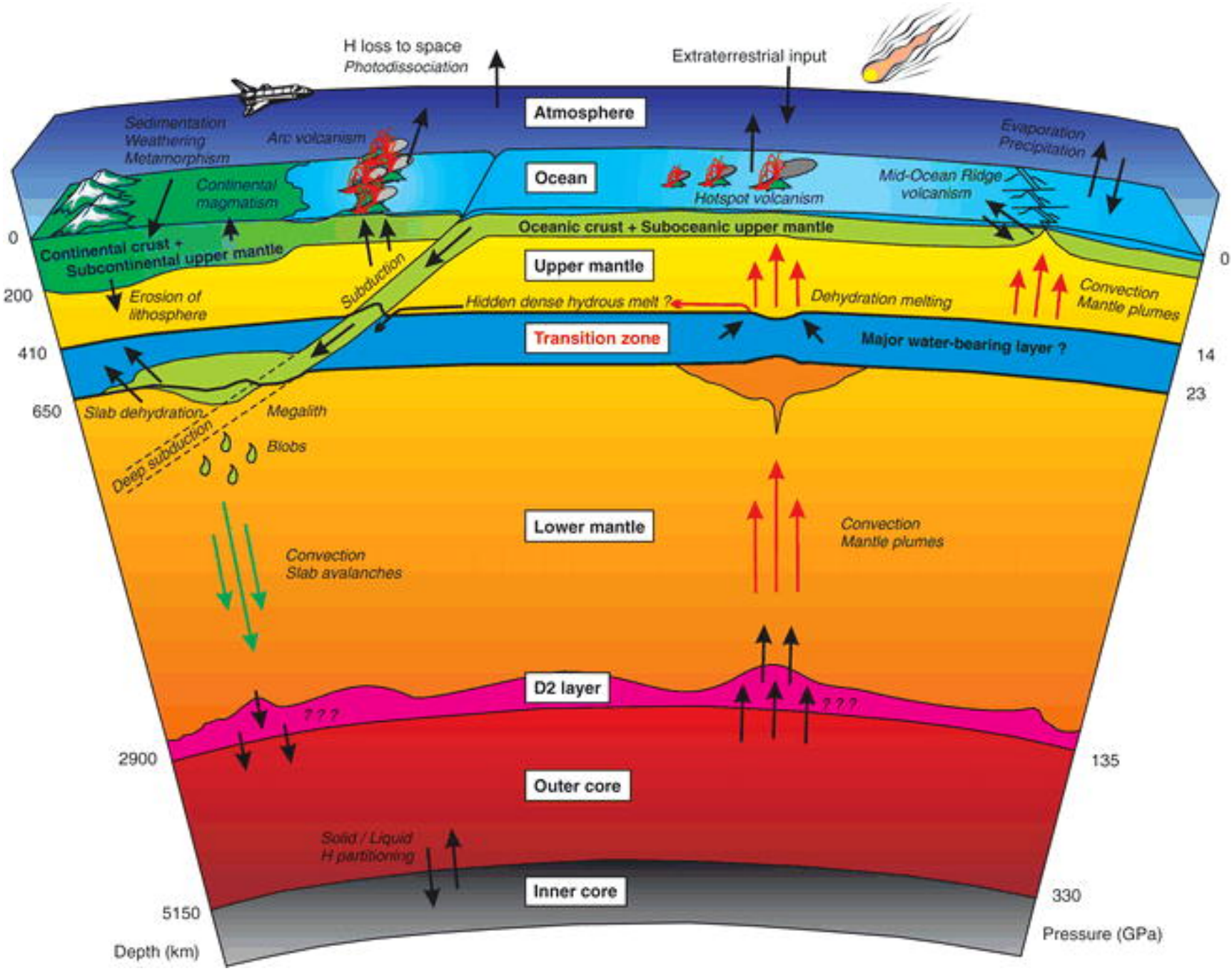
H loss to space
Photodissociation
Extraterrestrial input
Atmosphere
Ocean
Sedimentation
Weathering
Metamorphism
Arc volcanism
Continental magmatism
Hotspot volcanism
Mid-Ocean Ridge volcanism
Evaporation
Precipitation
Oceanic crust + Suboceanic upper mantle
Continental crust + Subcontinental upper mantle
Upper mantle
Subduction
Erosion of lithosphere
Hidden dense hydrous melt ?
Dehydration melting
Convection
Mantle plumes
Transition zone
Major water-bearing layer ?
Slab dehydration
Megalith
Deep subduction
Blobs
Lower mantle
Convection
Slab avalanches
Convection
Mantle plumes
D2 layer
? ? ?
? ? ?
Outer core
Solid / Liquid
H partitioning
Inner core
0
200
410
650
2900
5150
Depth (km)
0
14
23
135
330
Pressure (GPa)

Form of downwelling

- subduction
- delamination

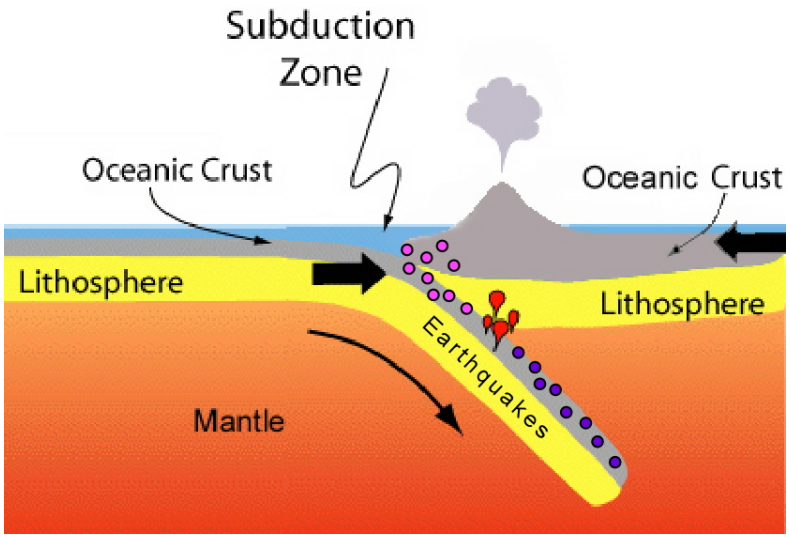

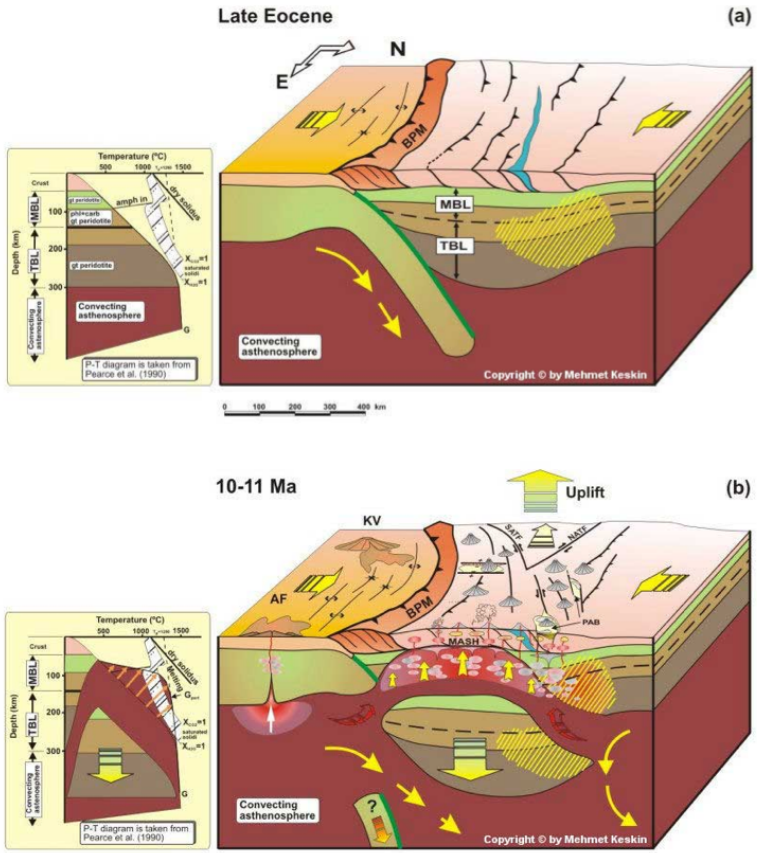

http://www.mantleplumes.org

Form of downwelling (2)

Delamination:

Small-scale convection at the edge of the Colorado Plateau: Implications for topography, magmatism, and evolution of Proterozoic lithosphere

J.W. van Wijk[1*], W.S. Baldridge[2], J. van Hunen[3], S. Goes[4], R. Aster[5], D.D. Coblentz[2], S.P. Grand[6], and J. Ni[7]

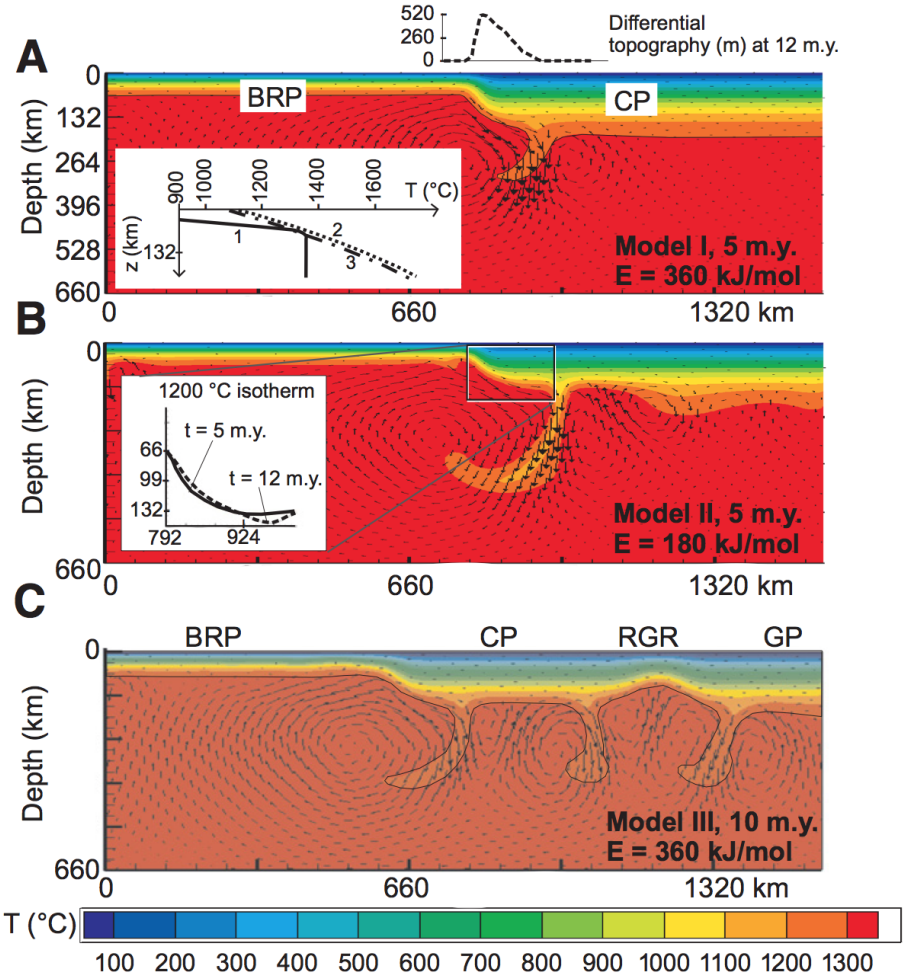

Form of upwelling

- accretional plate margins (spreading centers/mid-ocean ridges)
- mantle plumes

Form of upwelling

- accretional plate margins (spreading centers/mid-ocean ridges)
- mantle plumes

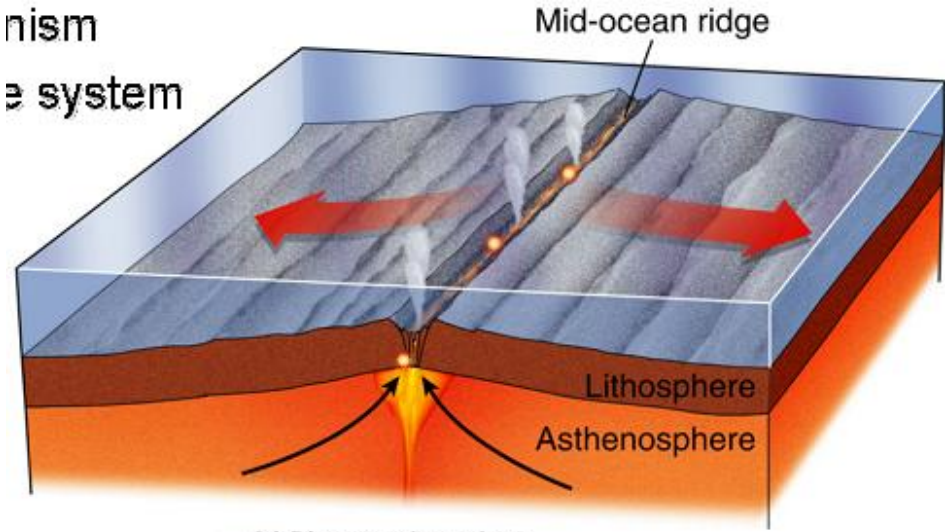

(a) Divergent boundary

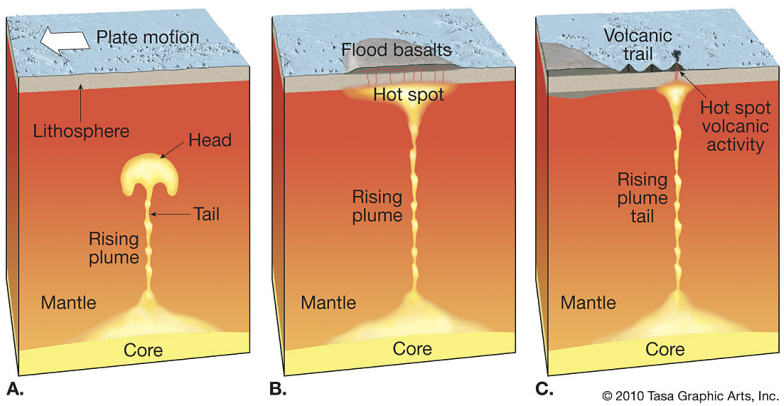

Mantle convection

- time dependent (highly time dependent / chaotic / turbulent)
- variable viscosity
- non-linear viscosity
- phase transformation
- compressibility

Compressibility is significant in mantle convection because the density of the Earth's mantle increases by 60% from the top to the bottom.
$\rightarrow$ Compressible vs incompressible ?

Physics of the Earth and Planetary Interiors, 25 (1981) 297–356
Elsevier Scientific Publishing Company, Amsterdam – Printed in The Netherlands

Preliminary reference Earth model *

Adam M. Dziewonski [1] and Don L. Anderson [2]

[1] *Department of Geological Sciences, Harvard University, Cambridge, MA 02138 (U.S.A.)*
[2] *Seismological Laboratory, California Institute of Technology, Pasadena, CA 91125 (U.S.A.)*

(Received December 3, 1980; accepted for publication December 5, 1980)

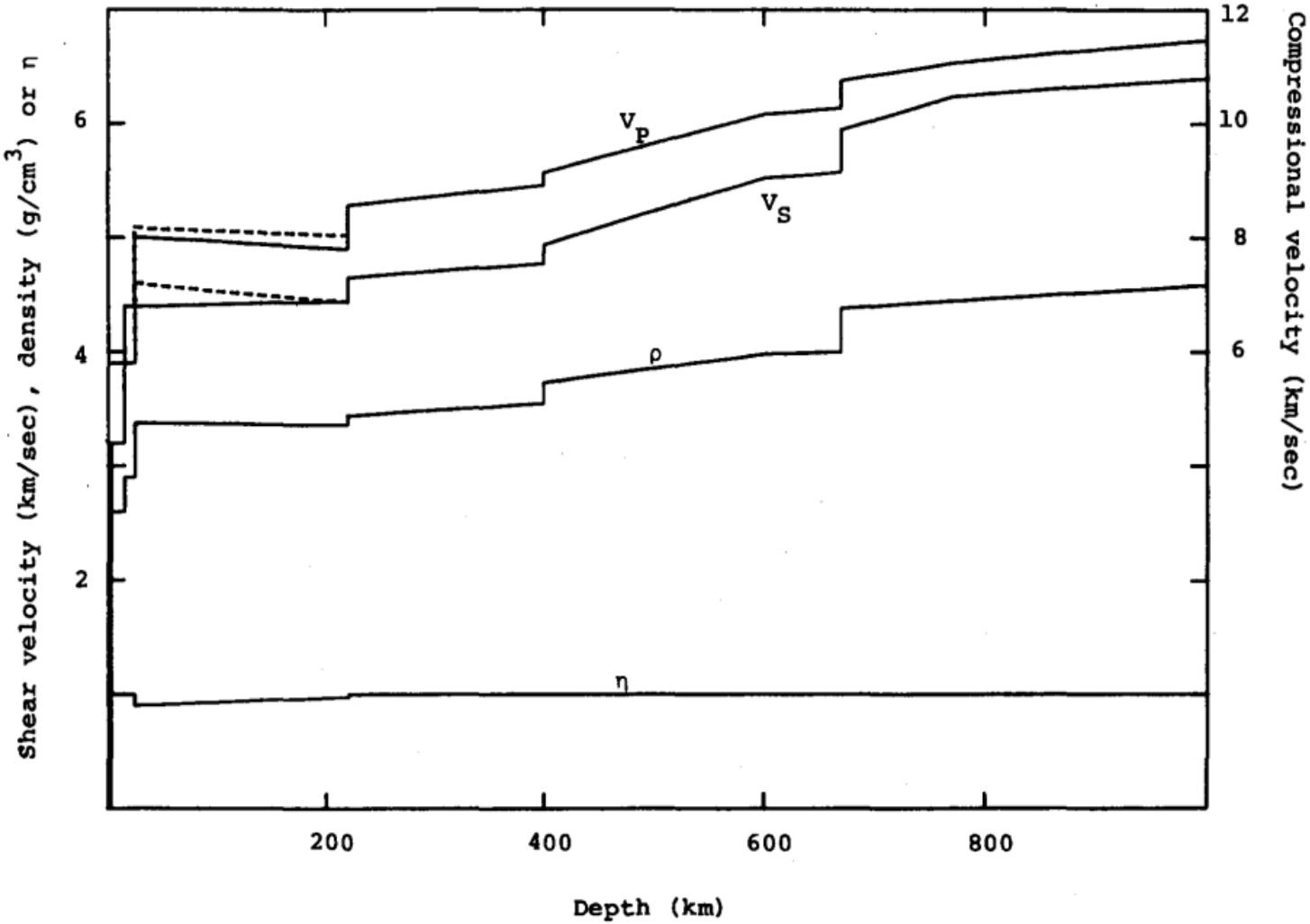

Compressible mantle convection ...
how hard can it be?

COMPUTATIONAL INFRASTRUCTURE FOR GEODYNAMICS (CIG)

ASPECT

Advanced Solver for Problems in Earth's ConvecTion

User Manual

Version 2.0.0-pre

(generated January 30, 2018)

Wolfgang Bangerth
Juliane Dannberg
Rene Gassmöller
Timo Heister

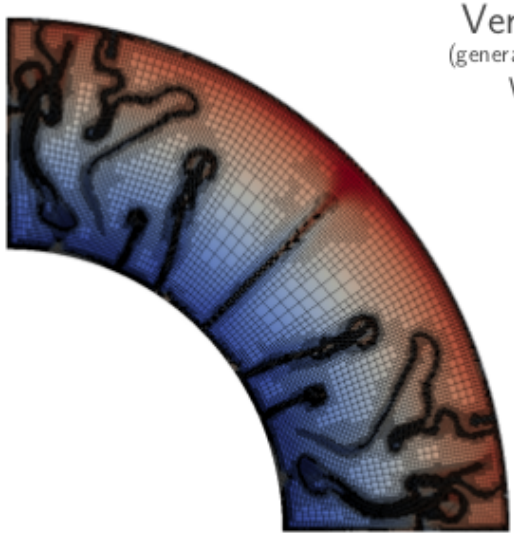

with contributions by:
Jacqueline Austermann, Markus Bürg, Samuel Cox, William Durkin, Grant Euen, Menno Fraters, Thomas Geenen, Anne Glerum, Ryan Grove, Eric Heien, Louise Kellogg, Scott King, Martin Kronbichler, Marine Lasbleis, Shangxin Liu, Elvira Mulyukova, John Naliboff, Jonathan Perry-Houts, Elbridge Gerry Puckett, Tahiry Rajaonarison, Ian Rose, D. Sarah Stamps, Cedric Thieulot, Iris van Zelst, Siqi Zhang

geodynamics.org

Let's have a look at the manual...

ASPECT solves a system of equations in a $d = 2$- or $d = 3$-dimensional domain Ω that describes the motion of a highly viscous fluid driven by differences in the gravitational force due to a density that depends on the temperature. In the following, we largely follow the exposition of this material in Schubert, Turcotte and Olson [STO01].

Specifically, we consider the following set of equations for velocity $\mathbf{u}$, pressure p and temperature T, as well as a set of advected quantities c_i that we call *compositional fields*:

$$-\nabla \cdot \left[2\eta \left(\varepsilon(\mathbf{u}) - \frac{1}{3}(\nabla \cdot \mathbf{u})\mathbf{1} \right) \right] + \nabla p = \rho \mathbf{g} \qquad \text{in } \Omega, \tag{1}$$

$$\nabla \cdot (\rho \mathbf{u}) = 0 \qquad \text{in } \Omega, \tag{2}$$

$$\begin{aligned} \rho C_p \left(\frac{\partial T}{\partial t} + \mathbf{u} \cdot \nabla T \right) - \nabla \cdot k \nabla T &= \rho H \\ &\quad + 2\eta \left(\varepsilon(\mathbf{u}) - \frac{1}{3}(\nabla \cdot \mathbf{u})\mathbf{1} \right) : \left(\varepsilon(\mathbf{u}) - \frac{1}{3}(\nabla \cdot \mathbf{u})\mathbf{1} \right) \\ &\quad + \alpha T \left(\mathbf{u} \cdot \nabla p \right) \\ &\quad + \rho T \Delta S \left(\frac{\partial X}{\partial t} + \mathbf{u} \cdot \nabla X \right) \qquad \text{in } \Omega, \end{aligned} \tag{3}$$

$$\frac{\partial c_i}{\partial t} + \mathbf{u} \cdot \nabla c_i = q_i \qquad \text{in } \Omega, i = 1 \ldots C \tag{4}$$

where $\varepsilon(\mathbf{u}) = \frac{1}{2}(\nabla \mathbf{u} + \nabla \mathbf{u}^T)$ is the symmetric gradient of the velocity (often called the *strain rate*).[1]

ASPECT solves a system of equations in a $d = 2$- or $d = 3$-dimensional domain Ω that describes the motion of a highly viscous fluid driven by differences in the gravitational force due to a density that depends on the temperature. In the following, we largely follow the exposition of this material in Schubert, Turcotte and Olson [STO01].

Specifically, we consider the following set of equations for velocity $\mathbf{u}$, pressure p and temperature T, as well as a set of advected quantities c_i that we call *compositional fields*:

$$-\nabla \cdot \left[2\eta\left(\varepsilon(\mathbf{u}) - \frac{1}{3}(\nabla\cdot\mathbf{u})\mathbf{1}\right)\right] + \nabla p = \rho \mathbf{g} \qquad \text{in } \Omega, \tag{1}$$

$$\nabla \cdot (\rho \mathbf{u}) = 0 \qquad \text{in } \Omega, \tag{2}$$

$$\begin{aligned} \rho C_p \left(\frac{\partial T}{\partial t} + \mathbf{u}\cdot\nabla T\right) - \nabla\cdot k\nabla T &= \rho H \\ &\quad + 2\eta\left(\varepsilon(\mathbf{u}) - \frac{1}{3}(\nabla\cdot\mathbf{u})\mathbf{1}\right) : \left(\varepsilon(\mathbf{u}) - \frac{1}{3}(\nabla\cdot\mathbf{u})\mathbf{1}\right) \\ &\quad + \alpha T\left(\mathbf{u}\cdot\nabla p\right) \\ &\quad + \rho T \Delta S \left(\frac{\partial X}{\partial t} + \mathbf{u}\cdot\nabla X\right) \qquad \text{in } \Omega, \end{aligned} \tag{3}$$

$$\frac{\partial c_i}{\partial t} + \mathbf{u}\cdot\nabla c_i = q_i \qquad \text{in } \Omega, i = 1\ldots C \tag{4}$$

where $\varepsilon(\mathbf{u}) = \frac{1}{2}(\nabla\mathbf{u} + \nabla\mathbf{u}^T)$ is the symmetric gradient of the velocity (often called the *strain rate*).[1]

$$\rho = \rho(\ldots)?$$

JOURNAL OF GEOPHYSICAL RESEARCH, VOL. 99, NO. B8, PAGES 15,919–15,938, AUGUST 10, 1994

Sensitivity of convection with an endothermic phase change to the form of governing equations, initial conditions, boundary conditions, and equation of state

Joel Ita

Seismological Laboratory, California Institute of Technology, Pasadena

Scott D. King

Department of Earth and Atmospheric Sciences, Purdue University, West Lafayette, Indiana

Abstract. Recent convection calculations have demonstrated that an endothermic phase transition can greatly decrease the vertical flow through the transition in a convecting system, in some cases leading to a layered flow. Using reasonable estimates of both the Rayleigh number and Clapeyron slope of the spinel to perovskite plus magnesiowüstite phase change, these results suggest that the 670-km phase change has a strong effect on mantle convection. This so-called "dynamic layering" phenomenon is further investigated with a compressible finite element code using a two-dimensional, Cartesian geometry. We find a weak sensitivity of the pattern of flow to the form of the equations, considering Boussinesq, extended Boussinesq, and anelastic compressible forms of the governing equations, assuming that the thermodynamic properties (thermal expansivity, heat capacity, and latent heat) remain constant. The pattern of flow, however, depends strongly on the initial conditions, boundary conditions and equation of state. We compare the simple equation-of-state formulations used in previous work with a self-consistent equation of state based on Debye and Birch-Murnaghan finite strain theory under a Mie-Grüneisen formulation. A thermal expansion coefficient that decreases monotonically with depth and is unaffected by changes in phase or temperature greatly enhances dynamic layering. This trend is reversed when the temperature, pressure, and phase dependence of thermodynamic properties such as thermal expansivity, entropy, and heat capacity is introduced. At moderate Rayleigh numbers, the pattern of the flow is strongly influenced by the pattern of the initial condition (i.e., the location of upwellings and downwellings); however, it is not sensitive to the thickness of the initial thermal boundary layers. The sensitivity of the flow to the pattern of the initial condition can potentially bias mass fluxes, especially for moderate Rayleigh number calculations.

Introduction

How, or whether, material is transported between the upper and lower mantle is a question with profound implications for Earth's thermal and chemical evolution. *Birch* [1952] recognized an anomalous region of seismic velocities in the mantle from 200 to 800 km which he called the transition zone. He suggested that the transition zone held the key to many geophysical problems. Recently, the center of attention has been the 670 km seismic discontinuity, where seismic velocities increase by about 6% over a few kilometers. Laboratory experiments demonstrate that the transformation from spinel to perovskite plus magnesiowüstite is endothermic and occurs at a pressure that is compatible with the depth of the 670-km seismic discontinuity [*Liu*, 1976; *Ito and Takahashi*, 1989; *Akaogi and Ito*, 1993] and the observed depression of the discontinuity in Benioff zones [*Wicks and Richards*, 1993]. While there is still considerable uncertainty in the measurements, the experimentally determined value of the Clapeyron slope is -3.0 ± 1.0 MPa/°K and occurs over a pressure range equivalent to a depth range of ≤ km in the mantle [*Akaogi and Ito*, 1993].

For an endothermic phase transition, the change in phase occurs at greater depths in cold, downgoing plumes (slabs) than in average, ambient mantle. The reverse is true for hot, upwelling plumes: the phase change occurs at shallower depths in the plume, providing a buoyancy force that counteracts the less dense, warmer plume material. The depression of the phase transition in the vicinity of the subducting slab causes a negative density anomaly (i.e., an upward force) that counteracts the downward buoyancy force of the cold slab. It is not hard to see that given a sufficiently large retarding force from the phase transition, the vertical descent of the

Abstract. Recent convection calculations have demonstrated that an endothermic phase transition can greatly decrease the vertical flow through the transition in a convecting system, in some cases leading to a layered flow. Using reasonable estimates of both the Rayleigh number and Clapeyron slope of the spinel to perovskite plus magnesiowüstite phase change, these results suggest that the 670-km phase change has a strong effect on mantle convection. This so-called "dynamic layering" phenomenon is further investigated with a compressible finite element code using a two-dimensional, Cartesian geometry. We find a weak sensitivity of the pattern of flow to the form of the equations, considering Boussinesq, extended Boussinesq, and anelastic compressible forms of the governing equations, assuming that the thermodynamic properties (thermal expansivity, heat capacity, and latent heat) remain constant. The pattern of flow, however, depends strongly on the initial conditions, boundary conditions and equation of state. We compare the simple equation-of-state formulations used in previous work with a self-consistent equation of state based on Debye and Birch-Murnaghan finite strain theory under a Mie-Grüneisen formulation. A thermal expansion coefficient that decreases monotonically with depth and is unaffected by changes in phase or temperature greatly enhances dynamic layering. This trend is reversed when the temperature, pressure, and phase dependence of thermodynamic properties such as thermal expansivity, entropy, and heat capacity is introduced. At moderate Rayleigh numbers, the pattern of the flow is strongly influenced by the pattern of the initial condition (i.e., the location of upwellings and downwellings); however, it is not sensitive to the thickness of the initial thermal boundary layers. The sensitivity of the flow to the pattern of the initial condition can potentially bias mass fluxes, especially for moderate Rayleigh number calculations.

Governing Equations

The equations derived from the principles of conservation of mass, momentum, and energy which govern convection in a very low Mach number, infinite Prandtl number fluid are [*Jarvis and McKenzie*, 1980]

$$\nabla \cdot (\rho \vec{v}) = 0 \tag{1}$$

$$0 = -\nabla P + \rho \vec{g} + \frac{\partial \tau_{ij}}{\partial x_j} \tag{2}$$

$$\rho \frac{Dq}{Dt} = \nabla \cdot (k \nabla T) + \rho H + \tau_{ij} \frac{\partial v_i}{\partial x_j}, \tag{3}$$

where D/Dt is the material derivative and the variables are defined in Table 1.

Using the thermodynamic relations

$$dq = TdS \tag{4}$$

and

$$dS = \frac{C_P}{T} dT - \frac{\alpha}{\rho} dP, \tag{5}$$

equation (3) can be rewritten as

$$\rho C_P \frac{DT}{Dt} - \alpha T \frac{DP}{Dt} =$$

$$\nabla \cdot (k \nabla T) + \rho H + \tau_{ij} \frac{\partial v_i}{\partial x_j}. \tag{6}$$

The effect of latent heat, q_L, of a phase transition can be introduced into equation (6) in two different ways. One method is to explicitly specify the variation in thermal expansivity and heat capacity due to the exchange of latent heat in addition to any pressure, temperature, or petrological variation [see *Zhao et al.*, 1992, and references therein]. Another tack is to introduce the latent heat directly into equation (3), which would then take the form

$$\rho C_P \frac{DT}{Dt} - \alpha T \frac{DP}{Dt}$$

$$= \nabla \cdot (k \nabla T) + \rho H + \tau_{ij} \frac{\partial v_i}{\partial x_j} + T \frac{DS_L}{Dt}, \tag{7}$$

where the latent heat has been expanded using the thermodynamic relation given above in equation (4). Thus S_L is the entropy change associated the latent heat q_L. In this case, only variations in thermal expansivity and heat capacity due to changes in pressure, temperature, or petrology are taken into account. Because density is calculated independently of thermal expansivity and heat capacity, equations (1) and (2) are uneffected by this representation.

When solving equations (1) and (2), the absolute pressure field is usually not determined. Instead, a reference density (and thus pressure) profile is assumed a priori. This reference profile is fixed through out the calculation. Given this assumption, our development will be altered in the following way. Introducing the expansions

$$P = P_r + P' \tag{8}$$

$$\rho = \rho_r(P_r) + \rho'(P', T), \tag{9}$$

where the subscript r denotes the reference value of the property it is associated with and the primed variables represent departures from the reference state, the equations for the conservation of momentum and energy become

$$0 = -\nabla P_r - \nabla P' + \rho_r \vec{g} + \rho' \vec{g} + \frac{\partial \tau_{ij}}{\partial x_j} \tag{10}$$

$$\rho C_P \frac{DT}{Dt} - \alpha T \left(\frac{DP'}{Dt} + \frac{\partial P_r}{\partial t} + \vec{v} \cdot \nabla P_r \right)$$

$$= \nabla \cdot (k \nabla T) + \rho H + \tau_{ij} \frac{\partial v_i}{\partial x_j} + \rho T \frac{DS_L}{Dt}. \tag{11}$$

The value of P_r is time independent and spatially variable only in the vertical direction, i.e.,

$$\frac{\partial P_r}{\partial t} = 0 \tag{12}$$

$$\nabla P_r = \frac{\partial P_r}{\partial z} \vec{e}_z = \rho_r \vec{g}. \tag{13}$$

Thus equations (10) and (11) become

$$\nabla P' = \rho' \vec{g} + \frac{\partial \tau_{ij}}{\partial x_j} \tag{14}$$

They include phase change as follows:

The effect of latent heat, q_L, of a phase transition can be introduced into equation (6) in two different ways. One method is to explicitly specify the variation in thermal expansivity and heat capacity due to the exchange of latent heat in addition to any pressure, temperature, or petrological variation [see *Zhao et al.*, 1992, and references therein]. Another tack is to introduce the latent heat directly into equation (3), which would then take the form

$$\rho C_P \frac{DT}{Dt} - \alpha T \frac{DP}{Dt}$$

$$= \nabla \cdot (k \nabla T) + \rho H + \tau_{ij} \frac{\partial v_i}{\partial x_j} + T \frac{DS_L}{Dt}, \qquad (7)$$

where the latent heat has been expanded using the thermodynamic relation given above in equation (4). Thus S_L is the entropy change associated the latent heat q_L. In this case, temperature gradient slightly, but a positive density gradient is introduced. The effect of an endothermic phase change in decreases the temperature locally, even though the density increases. Away from the thermal boundary layers, the temperature profile should closely resemble that of a volume element of fluid moving adiabatically within the cell.

Thermodynamic Properties and Equation of State

The thermodynamic properties (α, C_P, and S) and the pressure-volume-temperature equation of state of this physical system will be cast in two forms to determine the effect of the approximations of the equation of state on convective patterns. Most numerical studies of convection with a phase change use a formulation similar that of *Richter* [1973] where the progress function of the phase transition, π, is given by

$$\pi = \frac{1}{2}\left[1 + \tanh\left(\frac{P - P_t - \gamma(T - T_t)}{d}\right)\right], \qquad (21)$$

where γ is the Clapeyron slope of the phase transition, d is half the transition width at constant temperature, and the variable subscripted by t represents the value at the average depth of the phase transition. Under the BA and EBA form of the governing equations, density at any point in the convective system is then given by

$$\rho = \rho_o \left(1 - \alpha T + \frac{\pi \delta\rho}{\rho_o}\right), \qquad (22)$$

where $\delta\rho$ is the change in density across the phase transition.

Their conclusions:

While previous studies have clearly demonstrated that an endothermic phase change has a stronger effect on vertical flow with increasing Rayleigh number, we show that the initial conditions, boundary conditions, and equation of state approximations also have important effects on the evolution of a convecting system with an endothermic phase change at a moderate Rayleigh number. In particular, (1) at Rayleigh numbers of order 10^5, the initial flow pattern imposed on the system can persist for 30-40 transit times or more. (2) Reflecting sidewall boundary conditions used in a Cartesian, box-like system tend produce layered flows more easily than those with flow-through conditions. (3) A general increase in mass flux is seen as one increases the order of approximation of the governing equations from the BA to the EBA to the TALA. (4) Introducing temperature and phase variations in thermal expansivity can lead to a significant decrease in the impedance of flow across the phase boundary compared with models that assume a monotonic decrease in this property with depth. (5) Temperature variations in the latent heat of the transition can increase the impedance of flow through the boundary.

Gouverning equation

Commonly we find four types of equations used in the literature:

- Anelastic Liquid Approximation (ALA)
- Truncated Anelastic Liquid Approximation (TALA)
- Extended Boussinesq Approximation (EBA)
- Boussinesq Approximation (BA)

Scaling of the heat transport equation

$$\rho c_p \frac{DT}{dt} - \alpha T \rho \boldsymbol{v} \cdot \boldsymbol{g} = \boldsymbol{\nabla} \cdot (k \boldsymbol{\nabla} T) + \boldsymbol{s} : \boldsymbol{\nabla} \boldsymbol{v}$$

The usual scaling parameters for mantle convection are:

$$x = x' h_0 \qquad t = t' \frac{h_0^2}{\kappa_0} \qquad v = v' \frac{\kappa_0}{h_0} \qquad T = T' \Delta T$$

$$p = p' \frac{\mu_0 \kappa_0}{h_0^2} \qquad \rho = \rho' \rho_0 \qquad g = g' g_0 \qquad k = k' k_0 \qquad c_p = c_p' c_{p0} \qquad \alpha = \alpha' \alpha_0$$

The equation then rewrites:

$$(\rho' \rho_0)(c_p' c_{p0}) \frac{D(T' \Delta T)}{d(t' h_0^2/\kappa)} - (\alpha' \alpha_0)(T' \Delta T)(\rho' \rho_0)(\boldsymbol{v}' \frac{\kappa_0}{h_0}) \cdot (\boldsymbol{g}' g_0)$$

$$= \frac{1}{h_0^2} \boldsymbol{\nabla}' \cdot (k' k_0 \boldsymbol{\nabla}' (T' \Delta T)) + (\boldsymbol{s}' \frac{\mu_0 \kappa_0}{h_0^2}) : (\boldsymbol{\nabla}' \boldsymbol{v}' \frac{\kappa_0}{h_0^2})$$

which can be re-arranged:

$$\rho' c_p' \frac{DT'}{dt'} - (\alpha_0 g_0 h_0 / c_{p0}) \alpha' T' \rho' \boldsymbol{v}' \cdot \boldsymbol{g}' = \boldsymbol{\nabla} \cdot (k' \boldsymbol{\nabla}' T') + \frac{\mu_0 \kappa_0}{\rho_0 c_{p0} \Delta T h_0^2} \boldsymbol{s}' : \boldsymbol{\nabla}' \boldsymbol{v}'$$

Scaling of the heat transport equation

One can then define the *Dissipation number*

$$Di = \frac{\alpha_0 g_0 h}{c_{p0}}$$

and the *Rayleigh number*

$$Ra = \frac{\alpha_0 \rho_0 \Delta T g_0 h^3}{\mu_0 \kappa_0}$$

with

$$\frac{Di}{Ra} = \frac{\mu_0 \kappa_0}{\rho_0 c_{p0} \Delta T h_0^2}$$

so that finally:

$$\rho' c_p' \frac{DT'}{dt'} - Di \alpha' T' \rho' \boldsymbol{v}' \cdot \boldsymbol{g}' = \boldsymbol{\nabla} \cdot (k' \boldsymbol{\nabla}' T') + \frac{Di}{Ra} \boldsymbol{s}' : \boldsymbol{\nabla}' \boldsymbol{v}'$$

Scaling of the heat transport equation

One can then define the *Dissipation number*

$$Di = \frac{\alpha_0 g_0 h}{c_{p0}}$$

and the *Rayleigh number*

$$Ra = \frac{\alpha_0 \rho_0 \Delta T g_0 h^3}{\mu_0 \kappa_0}$$

with

$$\frac{Di}{Ra} = \frac{\mu_0 \kappa_0}{\rho_0 c_{p0} \Delta T h_0^2}$$

so that finally:

$$\rho' c_p' \frac{DT'}{dt'} - Di \alpha' T' \rho' \boldsymbol{v}' \cdot \boldsymbol{g}' = \boldsymbol{\nabla} \cdot (k' \boldsymbol{\nabla}' T') + \frac{Di}{Ra} \boldsymbol{s}' : \boldsymbol{\nabla}' \boldsymbol{v}'$$

For the Earths mantle,

- the dissipation number is between 0.25 and 0.8.
- the Rayleigh number is about 10^7

Looking at the literature

- Large body of work
- Models of increasing complexity
- developments go hand in hand with ever more powerful computers
- complicated physics/geochemistry $\rightarrow$ difficult numerics

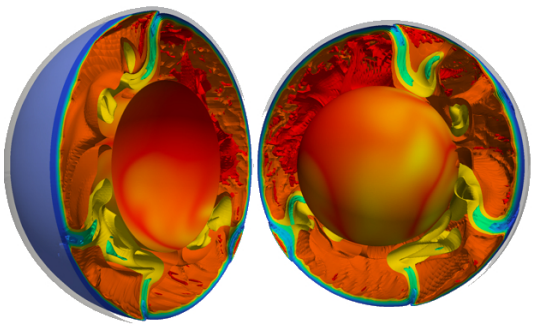

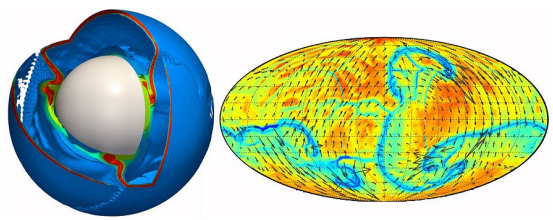

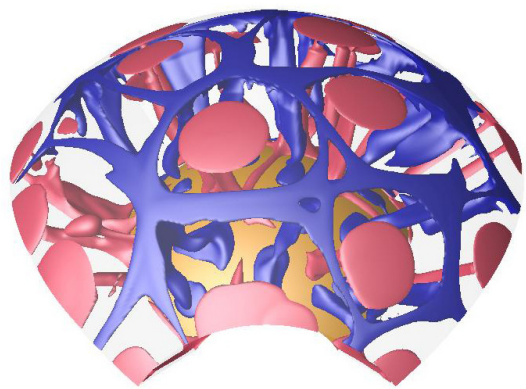

Earth-Science Reviews 110 (2012) 1–25

Contents lists available at SciVerse ScienceDirect

Earth-Science Reviews

journal homepage: www.elsevier.com/locate/earscirev

Dynamics and evolution of the deep mantle resulting from thermal, chemical, phase and melting effects

Paul J. Tackley *

Institute of Geophysics, Department of Earth Sciences, ETH Zürich, Sonneggstrasse 5, 8092 Zurich, Switzerland

ARTICLE INFO

Article history:
Received 22 June 2011
Accepted 3 October 2011
Available online 10 October 2011

Keywords:
Mantle convection
Core–mantle boundary
D″
Post-perovskite
Ultra-low velocity zone

ABSTRACT

The core–mantle boundary (CMB) – the interface between the silicate mantle and liquid iron alloy outer core – is the most important boundary inside our planet, with processes occurring in the deep mantle above it playing a major role in the evolution of both the core and the mantle. The last decade has seen an astonishing improvement in our knowledge of this region due to improvements in seismological data and techniques for mapping both large- and small-scale structures, mineral physics discoveries such as post-perovskite and the iron spin transition, and dynamical modelling. The deep mantle is increasingly revealed as a very complex region characterised by large variations in temperature and composition, phase changes, melting (possibly at present and certainly in the past), and anisotropic structures. Here, some fundamentals of the relevant processes and uncertainties are reviewed in the context of long-term Earth evolution and how it has led to the observed present-day structures. Melting has been a dominant process in Earth's evolution. Several processes involving melting, some of which operated soon after Earth's formation and some of which operated throughout its history, have produced dense, iron rich material that has likely sunk to the deepest mantle to be incorporated into a heterogeneous basal mélange (BAM) that is now evident seismically as two large low-velocity regions under African and the Pacific, but was probably much larger in the past. This BAM modulates core heat flux, plume formation and the separation of different slab components, and may contain various trace-element cocktails required to explain geochemical observations. The geographical location of BAM material has, however, probably changed through Earth's history due to the inherent time-dependence of plate tectonics and continental cycles.

Geophysical Journal International

Geophys. J. Int. (2010) **180,** 73–87 doi: 10.1111/j.1365-246X.2009.04413.x

A community benchmark for 2-D Cartesian compressible convection in the Earth's mantle

Scott D. King,[1] Changyeol Lee,[1] Peter E. van Keken,[2] Wei Leng,[3] Shijie Zhong,[3] Eh Tan,[4] Nicola Tosi[5,6] and Masanori C. Kameyama[7]

[1]*Department of Geosciences, Virginia Tech, Blacksburg,* VA 24061, *USA. E-mail: sdk@vt.edu*
[2]*Department of Geological Sciences, University of Michigan, Ann Arbor,* MI 48109, *USA*
[3]*Department of Physics, University of Colorado, Boulder,* CO 80309, *USA*
[4]*Seismological Laboratory, Caltech, Pasadena,* CA 91125, *USA*
[5]*Department of Geophysics, Faculty of Mathematics and Physics, Charles University, Prague, Czech Republic*
[6]*Institute of Geological Sciences, Freie Universität, Berlin, Germany*
[7]*Geodynamics Research Center (GRC), Ehime University, Matsuyama, Japan*

Accepted 2009 October 8. Received 2009 October 5; in original form 2009 June 19

SUMMARY

Benchmark comparisons are an essential tool to verify the accuracy and validity of computational approaches to mantle convection. Six 2-D Cartesian compressible convection codes are compared for steady-state constant and temperature-dependent viscosity cases as well as time-dependent constant viscosity cases. In general we find good agreement between all codes when comparing average flow characteristics such as Nusselt number and rms velocity. At Rayleigh numbers near 10^6 and dissipation numbers between 0 and 2, the results differ by approximately 1 per cent. Differences in discretization and use of finite volumes versus finite elements dominate the differences. There is a small systematic difference between the use of the anelastic liquid approximation (ALA) compared to that of the truncated ALA. In determining the onset of time-dependence, there was less agreement between the codes with a spread in the Rayleigh number where the first bifurcation occurs ranging from 7.79×10^5 to 1.05×10^6.

Key words: Numerical solutions; Numerical approximations and analysis; Equations of state; Dynamics of lithosphere and mantle.

1 INTRODUCTION

As pressure increases through the mantle there is a corresponding increase in density due to self-compression. In a vigorously convecting mantle, the rate at which mechanical energy is converted into heat (i.e. viscous dissipation) is non-negligible and contributes to the heat energy of the fluid, resulting in adiabatic temperature and density gradients that reduce the vigour of convection. In the non-dimensional form of the equations, the magnitude of the dissipation is controlled by a dimensionless parameter called the Dissipation number, *Di*. For the Earth's mantle, the effect of compressibility is moderate (Jarvis & McKenzie 1980) and the dissipation number is between 0.25 and 0.8. The majority of mantle convection studies have assumed an incompressible mantle where the dissipation number is assumed to be zero. However, viscous dissipation may interact with rheology and/or changes in composition and the effect on mantle dynamics and geophysical observations may be more significant than has been previously thought (e.g. King & Ita 1995; Ita & King 1998; Tan & Gurnis 2005, 2007; Leng & Zhong 2008; Lee & King 2009). In addition, the effect of compressibility on time-dependent flow has not be examined. Often an adiabatic gradient is added *a posteriori* to convection calculations to incorporate the effect of compressibility. However, this does not take into account the potential feedback between rheology and adiabatic heating (*cf.* Yuen *et al.* 1987). While there has been extensive benchmarking of incompressible mantle convection codes (Blankenbach *et al.* 1989; Travis *et al.* 1990; van Keken *et al.* 1997; Koglin *et al.* 2005; van Keken *et al.* 2008), there has been no compressible convection benchmark.

This paper grew out of a workshop on compressible convection held at Purdue University in 2006 March that was sponsored by the Computational Infrastructure for Geodynamics project (www.geodynamics.org). As in Blankenbach *et al.* (1989) we focus on a comparison of derived quantities from the temperature and velocity field that are predicted for a number of prescribed cases. The derived quantities include the Nusselt number *Nu* (non-dimensional average heat flow), and the non-dimensional root-mean-square (rms) velocity, volume averaged work and viscous dissipation. We did not compare computational efficiency given the different computer architectures that the contributing groups employed. Authors chose the grid resolution based on their experience with the codes and their desire to balance accuracy versus CPU time. We illustrate the effect of increasing grid resolution on one typical problem with one code. Many of the codes have previously

2 EQUATIONS

While the general, dimensional equations for a compressible fluid and various simplifying approximations have been presented elsewhere (e.g. Turcotte *et al.* 1974; Jarvis & McKenzie 1980; Ita & King 1994; Schubert *et al.* 2001; Leng & Zhong 2008), it is worth repeating them here again for clarity. The derivation below follows that in Schubert *et al.* (2001). Mass conservation is given by

$$\frac{\partial \rho}{\partial t} + \nabla \cdot (\rho \vec{u}) = 0, \tag{1}$$

where ρ is the density and $\vec{u}$ is the velocity. The conservation of momentum is given by,

$$\frac{\mathrm{D}\rho\vec{u}}{\mathrm{D}t} = -\nabla P + \nabla \cdot \tau + \rho\vec{g}, \tag{2}$$

where P is the pressure, $\vec{g}$ is the gravity, $\mathrm{D}/\mathrm{D}t$ is the material derivative, and τ is the deviatoric stress tensor given by,

$$\tau = 2\eta\dot{\epsilon} = \eta(\nabla\vec{u} + \nabla\vec{u}^T) - \frac{2}{3}\eta\nabla\cdot\vec{u}\delta_{ij}, \tag{3}$$

where η is the dynamic viscosity, $\dot{\epsilon}$ is the strain-rate tensor, and δ_{ij} is the Kroneker delta. Eq. (3) assumes that the bulk viscosity of the fluid is zero. Finally, the equation of energy conservation is given by,

$$\rho c_p \frac{\mathrm{D}T}{\mathrm{D}t} - \alpha T \frac{\mathrm{D}P}{\mathrm{D}t} = \nabla \cdot (k\nabla T) + \rho H + \phi, \tag{4}$$

where T is the temperature, c_p is the heat capacity at constant pressure, α is the coefficient of thermal expansion, k is the thermal conductivity, H is the volumetric heat production and ϕ is the viscous dissipation given by,

$$\phi = \frac{1}{2}\tau : \dot{\epsilon} = \tau_{ij}\frac{\partial u_i}{\partial x_j}. \tag{5}$$

In compressible convection, there is the additional required assumption—the reference state,

$$T = \bar{T} + T' \tag{6}$$

$$P = \bar{p} + p' \tag{7}$$

$$\rho = \bar{\rho}(\bar{T}, \bar{p}) + \rho', \tag{8}$$

where the overbarred quantities are time-independent and functions of depth only. The reference pressure is given by the hydrostatic approximation,

$$\nabla\bar{p} = \bar{\rho}g. \tag{9}$$

Using the assumption that $p' \ll \bar{p}$, we can eliminate pressure from the energy eq. (4), yielding

$$\begin{aligned}\rho c_p \frac{\mathrm{D}T'}{\mathrm{D}t} &= \nabla \cdot [k\nabla(T' + \bar{T})] + \rho H + \phi - \rho c_p \vec{u} \cdot \nabla\bar{T} \\ &\quad - \alpha(\bar{T} + T')\bar{\rho}gw,\end{aligned} \tag{10}$$

where $\vec{u} \cdot \vec{g} = -wg$, where w is the upward component of velocity.

For the reference state $(\bar{\rho}, \bar{T})$, we assume an adiabatic Adams–Williamson equation of state (Birch 1952), where

$$\bar{\rho}(z) = \rho_r \exp\left(\frac{\alpha_r g_r}{\gamma_r c_{p_r}} z\right), \quad \bar{T}(z) = T_{\mathrm{surf}} \exp\left(\frac{\alpha_r g_r}{c_{p_r}} z\right), \tag{11}$$

where z is the depth coordinate (parallel to the direction of gravity), γ_r is the reference value for the Grüneisen parameter, T_{surf} is the surface temperature, and variables with the subscript r are constant values used in defining the reference state. From this reference state, we note that $\nabla\bar{T} = (0, -\alpha_r g_r \bar{T}/c_{p_r})$, which along with dropping terms with ρ' and that $c_p \approx c_{p_r}$, allows us to further simplify the energy eq. (10),

$$\bar{\rho}\bar{c}_{p_r}\frac{\mathrm{D}T'}{\mathrm{D}t} = \nabla \cdot [k\nabla(T' + \bar{T})] + \bar{\rho}H + \phi - \bar{\rho}\bar{\alpha}gwT'. \tag{12}$$

The expansivity $\bar{\alpha}$ is $\frac{\alpha}{\alpha_r}$ and formally dependent on the reference state. For the purposes of the benchmark we will assume that $\bar{\alpha} = 1$.

2.1 Equations under the anelastic liquid approximation (ALA)

We non-dimensionalize the equations using the reference values for density, ρ_r, thermal expansivity, α_r, temperature contrast, ΔT_r, thermal conductivity, k_r, heat capacity, c_p, once again assuming that $c_p \approx c_{p_r}$ depth of the fluid layer, L and viscosity, η_r. The non-dimensionalization for velocity, u_r, pressure, p_r and time, t_r, become

$$u_r = \frac{k_r}{\rho_r c_p L}, \quad p_r = \frac{\eta_r k_r}{\rho_r c_p L^2}, \quad t_r = \frac{\rho_r c_p L^2}{k_r}. \tag{13}$$

The non-dimensionalization introduces four non-dimensional numbers, the Prandtl number, Pr, the Mach number, M, the dissipation number, Di and the Rayleigh number, Ra. If we assume that the relative volume change due to temperature, $\alpha_r \, \Delta T_r \ll 1$, $M^2 \, Pr \ll 1$ and $Pr \to \infty$, we arrive at the ALA.

Under the ALA, the conservation of mass becomes,

$$\nabla \cdot (\bar{\rho}\vec{u}) = 0, \tag{14}$$

the conservation of momentum becomes,

$$0 = -\nabla p' + \nabla \cdot \tau + Di \frac{\bar{\rho} c_p \hat{g}}{K_s \gamma_r c_v} p' - Ra \bar{\rho} \bar{\alpha} \hat{g} T' / \Delta T_r, \tag{15}$$

where $\hat{g}$ is the unit vector in the direction of gravity, c_v is the specific heat at constant volume, $\bar{\rho}$ is now dimensionless [i.e. eq. (11) divided by ρ_r] and the Rayleigh number and dissipation number are given by

$$Ra = \frac{\alpha_r \Delta T_r {\rho_r}^2 g_r L^3 c_p}{\eta_r k_r}, \; Di = \frac{\alpha_r g_r L}{c_p}. \tag{16}$$

With the assumption of constant thermal conductivity, and using the dimensionless reference states for $\bar{\rho}$ and $\bar{T}$ given by

$$\bar{\rho} = \rho_r \exp(z' Di/\gamma_r), \text{ and } \bar{T} = \frac{T_{\text{surf}}}{\Delta T_r} \exp(z' Di), \tag{17}$$

where z' is the dimensionless vertical coordinate. The conservation of energy (12) under the ALA becomes,

$$\bar{\rho} c_p \frac{DT'}{Dt} + Di \bar{\rho} \bar{\alpha} w T' = \nabla^2 T' + \bar{\rho} H + \phi \frac{Di}{Ra} + Di^2 \bar{T}. \tag{18}$$

Effects from equation of state and rheology in dissipative heating in compressible mantle convection

David A. Yuen*, Francesca Quareni†§ & H.-J. Hong‡

* Minnesota Supercomputer Institute and Department of Geology and Geophysics, University of Minnesota, Minneapolis, Minnesota 55455, USA
† Dipartimento di Fisica, Settore di Geofisica, Università di Bologna, 40127 Bologna, Italy
‡ Institute of Geology, State Seismological Bureau, Beijing, People's Republic of China
§ Present address: Istituto Nazionale di Geofisica Sezione di Bologna, Italy

The thermal profile in the Earth's interior is influenced by many factors. One of the least understood and studied processes is that resulting from adiabatic heating and viscous dissipation. With the exception of the work by Jarvis and McKenzie[1] very little has been done on the effects of compressibility on mantle circulation. It is quite common for geophysicists to add the adiabatic temperature gradient *a posteriori*[2] to temperature profiles derived from Boussinesq (incompressible) equations. Recently it has been shown[3] with the mean-field method[4] that there exists a strong coupling between the rheological parameters, such as the activation volume, and the thermodynamic constants governing adiabatic heating. Here we point out the important consequences brought about by incorporating the effects of equations of state and rheology in the dissipative heating term of the energy equation. We demonstrate explicitly the ways in which compression may raise the interior mantle temperature and illustrate how this effect can, in turn, be used for constraining some of the intrinsic parameters associated with the equation of state in the mantle.

We have employed the mean-field equations for studying steady-state behaviour, which should yield important information about the basic physics of the processes involved. Although it is an approximation to the full set of convective equations, the mean-field approach has increasingly been used by geophysicists to obtain preliminary ideas about various convection problems, ranging from variable-viscosity[5] to double-diffusive convection[6].

We have derived the single-mode, mean-field equations appropriate for an elastic, compressible convection[1] with variable viscosity in the limit of infinite Prandtl number. Within the present approximation, viscosity depends on horizontally averaged temperature and pressure. A depth-dependent equation of state $\rho(z)$, which increases exponentially with depth, is used for prescribing the background density profile. We have non-dimensionalized, with respect to the whole mantle, depth d ($d = 3{,}000$ km) and have chosen a z-axis pointing downward. The relevant steady-state equations may be written as the momentum equation

$$\frac{d^4W}{dz^4} + 2\frac{d^3W}{dz^3}\left(\frac{1}{\eta}\frac{d\eta}{dz} - 2\frac{D}{\gamma}\right) + \frac{d^2W}{dz^2}\left(\frac{1}{\eta}\frac{d^2\eta}{dz^2} - 5\frac{D}{\gamma}\frac{1}{\eta}\frac{d\eta}{dz} + 5\frac{D^2}{\gamma^2} - 2k^2\right) + \frac{dW}{dz}\left(3\frac{D^2}{\gamma^2}\frac{1}{\eta}\frac{d\eta}{dz} - \frac{D}{\gamma}\frac{1}{\eta}\frac{d^2\eta}{dz^2} - 2k^2\frac{1}{\eta}\frac{d\eta}{dz} - 2\frac{D^3}{\gamma^3} + 4k^2\frac{D}{\gamma}\right) + k^2W\left(\frac{1}{\eta}\frac{d^2\eta}{dz^2} + k^2 + \frac{D}{\gamma}\frac{1}{\eta}\frac{d\eta}{dz} - \frac{2}{3}\frac{D^2}{\gamma^2}\right) + k^2\exp\left(2\frac{D}{\gamma}z\right)R\frac{\theta}{\eta} = 0 \quad (1)$$

The temperature field is decomposed into a horizontally averaged part $\bar{T}(z)$ and a fluctuating component $\theta(z)\cos kx$, where k is the dimensionless wavenumber of the assumed roll along the x-direction. The equations for the mean and fluctuating temperatures in which the weak-coupling approximation[4] is assumed for the divergence of $u\theta - \langle u\theta\rangle$, take the form

$$\frac{1}{\rho(z)}\frac{d^2\bar{T}}{dz^2} - \frac{d}{dz}(\theta W) + D\theta W + \mu + \frac{D\eta}{R}\exp\left(-3\frac{D}{\gamma}z\right)\left[\left(2\frac{dW}{dz} + \frac{D}{\gamma}W\right)^2 + k^2\left(W + \frac{1}{k^2}\frac{D}{\gamma}\frac{d\theta}{dz} - \frac{1}{k^2}\frac{d^2W}{dz^2}\right)^2 + \frac{1}{3}\left(\frac{D}{\gamma}W\right)^2\right] = 0 \quad (2)$$

and

$$\frac{1}{\rho(z)}\left(\frac{d^2\theta}{dz^2} - k^2\theta\right) + D(\bar{T} + \bar{T}_0)W - W\frac{d\bar{T}}{dz} = 0 \quad (3)$$

In equations (1)–(3), the mean viscosity profile is given by η. The Rayleigh number R is based on the interior viscosity η_∞. The parameters D and γ are respectively the dissipation number and Grueneisen parameter associated with the equation of state[1] which is

$$\rho(z) = \rho_0 \exp(D/\gamma)z, \quad (4)$$

where ρ_0 is the surface density. The scale-height for the adiabatic temperature is given by $1/D$, whereas that for the density is

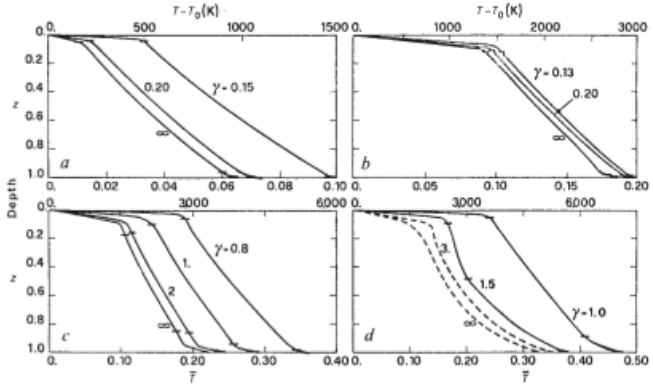

Fig. 1 Mean temperature as a function of depth for various rheologies. *a*, Constant viscosity, $\eta = \eta_\infty$; *b*, temperature-dependent viscosity, $\eta(\bar{T})$; *c* and *d*, temperature- and pressure-dependent viscosity, $\eta(\bar{T}, p)$. A heat flux, based on the conduction flux from volumetric heating with strength H, is imposed at the bottom. The Rayleigh number for variable viscosity is based on the asymptotic viscosity η_∞, and is 10^9 for all cases. The temperature has been non-dimensionalized by $\bar{T} = T - T_0/T_D$ where $T_D = \rho_0 H d^2/k_0$. The density ρ_0 is set to 3,400 kg m^{-3}, $H = 10^{-12}$ W kg^{-1} and $k_0 = 4$ W m^{-1} K^{-1}. The surface temperature T_0 is set to 1,100 K for all cases to simulate the effects of lithospheric lid from variable viscosity. $D = 0.5$ and $\mu = 0$. The rheological parameters correspond to $Q^* = 50$ kcal mol^{-1} in *b*, *c* and *d*, $V^* = 4$ cm^3 mol^{-1} in *c* and $v^* = 8$ cm^3 mol^{-1} in *d*. An aspect ratio of one is asumed for the convective roll.

The thermal profile in the Earth's interior is influenced by many factors. One of the least understood and studied processes is that resulting from adiabatic heating and viscous dissipation. With the exception of the work by Jarvis and McKenzie[1] very little has been done on the effects of compressibility on mantle circulation. It is quite common for geophysicists to add the adiabatic temperature gradient *a posteriori*[2] to temperature profiles derived from Boussinesq (incompressible) equations. Recently it has been shown[3] with the mean-field method[4] that there exists a strong coupling between the rheological parameters, such as the activation volume, and the thermodynamic constants governing adiabatic heating. Here we point out the important consequences brought about by incorporating the effects of equations of state and rheology in the dissipative heating term of the energy equation. We demonstrate explicitly the ways in which compression may raise the interior mantle temperature and illustrate how this effect can, in turn, be used for constraining some of the intrinsic parameters associated with the equation of state in the mantle.

the equation of state parameters can be estimated with greater precision.

We conclude that the coupling between variable viscosity and equation of state in dissipative heating is potentially an important mechanism in mantle convection. The fundamental concept that rheology, equation of state and radiogenic heating are all linked to each other by virtue of nonlinear thermomechanical couplings must be strongly emphasized as a consequence of these findings. To explore further the implications of this phenomenon for the Earth's thermal behaviour, we need to corroborate these results with the full equations and also with depth-dependent thermal expansion coefficient and thermal conductivity, which would have important implications for the D^{11} layer. With the next generation of supercomputers, the spatial resolution required to understand this nonlinear process in two or three dimensions is well attainable.

Support of this research has come from NSF grant EAR-8511200 and NASA grant NAG 5-770.

J. Fluid Mech. (1992), *vol.* 239, *pp.* 683–719
Printed in Great Britain

Three-dimensional convection of an infinite-Prandtl-number compressible fluid in a basally heated spherical shell

By DAVID BERCOVICI[1], GERALD SCHUBERT[2] AND GARY A. GLATZMAIER[3]

[1] Department of Geology and Geophysics, School of Ocean and Earth Science and Technology, University of Hawaii, Honolulu, HI 96822, USA

[2] Department of Earth and Space Sciences, University of California, Los Angeles, CA 90024, USA

[3] Earth and Environmental Sciences Division, Los Alamos National Laboratory, NM 87545, USA

(Received 10 November 1989 and in revised form 13 December 1991)

A numerical investigation is made of the effects of compressibility on three-dimensional thermal convection in a basally heated, highly viscous fluid spherical shell with an inner to outer radius ratio of approximately 0.55, characteristic of the Earth's whole mantle. Compressibility is implemented with the anelastic approximation and a hydrostatic adiabatic reference state whose bulk modulus is a linear function of pressure. The compressibilities studied range from Boussinesq cases to compressibilities typical of the Earth's whole mantle. Compressibility has little effect on the spatial structure of steady convection when the superadiabatic temperature drop across the shell ΔT_{sa} is comparable to a characteristic adiabatic temperature. When ΔT_{sa} is approximately an order of magnitude smaller than the adiabatic temperature, compressibility is significant. For all the non-Boussinesq cases, the regular polyhedral convective patterns that exist at large ΔT_{sa} break down at small ΔT_{sa} into highly irregular patterns; as ΔT_{sa} decreases convection becomes penetrative in the upper portion of the shell and is strongly time dependent at Rayleigh numbers only ten times the critical Rayleigh number, $\langle Ra \rangle_{cr}$. Viscous heating in the compressible solutions is concentrated around the upwelling plumes and is greatest near the top and bottom of the shell. Solutions with regular patterns (and large ΔT_{sa}) remain steady up to fairly high Rayleigh numbers ($100\langle Ra \rangle_{cr}$), while solutions with irregular convective patterns are time dependent at similar Rayleigh numbers. Compressibility affects the pattern evolution of the irregular solutions, producing fewer upwelling plumes with increasing compressibility.

1. Introduction

Convective flow in the Earth's mantle has been the subject of extensive research because of its relevance to plate tectonics and the structure and evolution of the terrestrial planets (Oxburgh & Turcotte 1978; Schubert 1979; Schubert, Stevenson & Stevenson & Cassen 1980; Olson, Silver & Carlson 1990). Evidence for convection exists in the directly measurable motions of the tectonic plates at the Earth's surface (Minster & Jordan 1978, 1987; Kroger *et al.* 1987), and in the correlations of seismically and gravitationally inferred mantle heterogeneities and core–mantle boundary topography with tectonic features (Runcorn 1967; Dziewonski 1984;

A numerical investigation is made of the effects of compressibility on three-dimensional thermal convection in a basally heated, highly viscous fluid spherical shell with an inner to outer radius ratio of approximately 0.55, characteristic of the Earth's whole mantle. Compressibility is implemented with the anelastic approximation and a hydrostatic adiabatic reference state whose bulk modulus is a linear function of pressure. The compressibilities studied range from Boussinesq cases to compressibilities typical of the Earth's whole mantle. Compressibility has little effect on the spatial structure of steady convection when the superadiabatic

GEOPHYSICAL RESEARCH LETTERS, VOL. 16, NO. 7, PAGES 633-636, JULY 1989

COMPRESSIBLE CONVECTION IN THE EARTH'S MANTLE: A COMPARISON OF DIFFERENT APPROACHES

Volker Steinbach, Ulrich Hansen, Adolf Ebel

Institut f. Geophysik und Meterologie, Universität zu Köln, F.R. Germany

Abstract. Numerical models of mantle convection using the Boussinesq, extended Bousinessq and anelastic-liquid approximation are compared. For steady state solutions there is good quantitative agreement between the results if they are scaled in a proper way. Time-dependent extended Boussinesq and anelastic-liquid flows show only qualitative agreement, the main difference being a distortion of timescale. Compressibility induces an asymmetry in the structure of upper and lower boundary layers that cannot be observed in Boussinesq fluids.

It has been argued that αK_s is almost constant in the lower mantle (e.g. Anderson, 1979), but recent high pressure - high temperature measurements (Boehler et al., 1989) give some evidence that this quantity decreases with pressure. According to these data, we used the relations $\alpha \sim \rho^{-6}$, $K_s \sim \rho^3$, leading to the (dimensionless) functions:

$$\rho = f^{1/2},\ \alpha = f^{-3},\ \gamma = f^{-2}, f = (1 + 2(D_0/\gamma_0)z), \quad (3)$$

where subscripts 0 denote zero pressure values.

GEOPHYSICAL RESEARCH LETTERS, VOL. 20, NO. 20, PAGES 2187-2190, OCTOBER 22, 1993

EFFECTS OF STRONGLY TEMPERATURE-DEPENDENT VISCOSITY ON TIME-DEPENDENT, THREE-DIMENSIONAL MODELS OF MANTLE CONVECTION.

Paul J Tackley

Seismological Laboratory, California Institute of Technology

Abstract. Numerical simulations of thermal convection in a wide (8x8x1) Cartesian box heated from below with temperature-dependent viscosity contrasts of 1000, and Rayleigh number 10^5 show that boundary conditions and aspect ratio have an enormous effect on the preferred flow pattern. With rigid upper and lower boundaries, spoke-pattern flow with small (diameter ~ 1.5) cells is obtained, consistent with laboratory experiments and previous numerical results. However, with the arguably more realistic stress-free boundaries, the flow chooses the largest possible wavelength, forming a single square cell of aspect ratio 8, with one huge cylindrical downwelling surrounded by upwelling sheets. The addition of stress-dependence to the rheology weakens the stiff upper boundary layer, resulting in smaller cells, though still with upwelling sheets and downwelling plumes.

Introduction

Increasingly realistic numerical models of three-dimensional (3-D) thermal convection in planetary mantles have been published in recent years, with Rayleigh numbers approaching that of the Earth, and various other complexities such as spherical geometry, depth-dependent properties, and mineralogical phase changes [Bercovici et al., 1989; Balachandar et al., 1992; Tackley et al., 1993]. However, by far the largest approximation in these calculations is the assumption of viscosity which is constant, or only depth-dependent. The viscosity of the Earth's mantle is known to be very strongly temperature dependent, resulting in the formation of rigid surface plates, and strongly modulating the characteristics of other proposed features, such as plumes from the core-mantle boundary. Thus, it is essential to incorporate such rheology into numerical models.

Laboratory experiments have given some insights into variable viscosity convection, but are limited in their applicability to the Earth by the use of rigid boundary conditions, since the mobility ofplates on the Earth suggests that stress-free boundary conditions are appropriate. White [1988] determined that the spoke-pattern is prefered for rigid boundary conditions, Rayleigh numbers above about 25000 and large viscosity variations.

Numerical work has mainly focussed on steady-state solutions in small boxes. Ogawa et al. [1992] modeled viscosity contrasts of up to 10^3, identifying the stagnant lid regime, characterized by upwelling plumes and downwelling sheets beneath a stagnant lid, and the whole-mantle regime, characterized by up- and down-welling plumes with sheet-like extensions. Christensen and Harder [1991] determined that in small boxes (aspect ratio up to 1.5) temperature-dependent viscosity favors upwelling plumes and downwelling sheets. They also obtained a spoke-pattern solution for rigid boundary conditions in a 4x4x1 box with viscosity contrasts of 30. Perhaps the most prophetic result was obtained by Weinstein and Christensen [1991], who, in the same 4x4x1 box, found that simply changing the upper boundary condition to stress-free resulted in a much longer wavelength pattern consisting of upwelling sheets and a downwelling plume.

In order to understand the Earth's mantle, it is important to determine the flow patterns with stress-free boundaries at both top and bottom, with large viscosity contrasts, and in a box whose aspect ratio is similar to the effective aspect ratio of the Earth's mantle. Here, solutions with these characteristics are presented.

Model

In order to isolate the effect of variable viscosity, the Boussinesq approximation is assumed, with all coefficients constant except viscosity. The infinte Prandtl number equations, non-dimensionalized to thermal diffusion timescale (D^2/κ), mantle depth (D), and superadiabatic temperature drop (ΔT), are as follows:

$$\nabla \cdot \underline{v} = 0 \tag{1}$$

$$\nabla \cdot \underline{\tau} - \nabla p = Ra_{1/2} T \underline{z} \tag{2}$$

$$\tau_{ij} = \eta(v_{i,j}+v_{j,i}) \tag{3}$$

$$\partial T/\partial t = \nabla^2 T - \nabla \cdot (\underline{v} T) \tag{4}$$

where $\underline{v}$, p, T, $\underline{\tau}$, and η are velocity, dynamic pressure, temperature (varying from 0 at the top boundary to 1 at the base), deviatoric stress and dynamic viscosity, respectively, $\underline{z}$ is a unit vector in the vertical direction, and the Rayleigh number $Ra_{1/2}$ is defined using the viscosity at T=0.5 as follows:

$$Ra_{1/2} = \rho g \alpha \Delta T D^3 / \eta_{1/2} \kappa \tag{5}$$

where ρ=density, g=gravitational acceleration, α=thermal expansivity and κ=thermal diffusivity. Viscosity is described by an Arrhenius law:

$$\eta_{New}(T) = \exp(13.8155(1/(T+1)-1/1.5)) \tag{6}$$

giving a variation between 100 and 0.1, with $\eta(0.5) = 1.0$

For the stress-dependence case:

$$\eta_{non\text{-}New} = \eta_{New}^{1/n} \dot{e}^{1/n-1} \sigma_0^{1-1/n} \tag{7}$$

$$\eta_{eff} = 2 (\eta_{New}^{-1} + \eta_{non\text{-}New}^{-1})^{-1} \tag{8}$$

where n is the power-law index, $\dot{e}$ is the strain rate and σ_0 is a

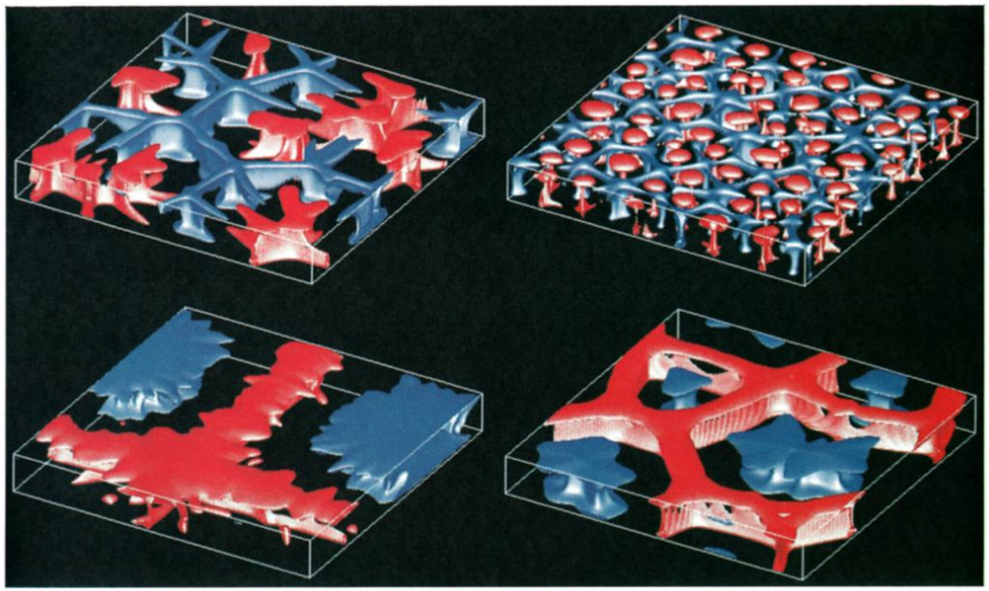

Fig. 1. Isocontours of residual temperature, showing where the temperature is higher (red) or lower (blue) than the horizontally-averaged value, by ±0.15 except where stated: a) (top left) Case 1, b) (top right) Case 2, c) (bottom left) Case 3, red contour is +0.1, d) (bottom right) Case 4, contours are ±0.1

Conclusions

These results show clearly the importance of stress-free boundary conditions and wide domains in understanding mantle convection with temperature-dependent viscosity. Very large cells are formed, with upwelling sheets and downwelling plumes, in contrast to the small-wavelength spoke pattern obtained with rigid boundary conditions. Although deep upwelling below mid-ocean ridges is suggested, the robustness of these patterns to internal heating, depth-dependent properties, spherical geometry and higher Rayleigh number needs to be established.

JOURNAL OF GEOPHYSICAL RESEARCH, VOL. 101, NO. B2, PAGES 3311–3332, FEBRUARY 10, 1996

Effects of strongly variable viscosity on three-dimensional compressible convection in planetary mantles

Paul J. Tackley[1]

Seismological Laboratory, California Institute of Technology, Pasadena

Abstract. A systematic investigation into the effects of temperature dependent viscosity on three-dimensional compressible mantle convection has been performed by means of numerical simulations in Cartesian geometry using a finite volume multigrid code, with a factor of 1000-2500 viscosity variation, Rayleigh numbers ranging from 10^5-10^7, and stress-free upper and lower boundaries. Considerable differences in model behavior are found depending on the details of rheology, heating mode, compressibility, and boundary conditions. Parameter choices were guided by realistic Earth models. In Boussinesq, basally heated cases with viscosity solely dependent on temperature and stress-free, isothermal boundaries, very long wavelength flows (~25,000 km, assuming the depth corresponds to mantle thickness) with cold plumes and hot upwelling sheets result, in contrast to the upwelling plumes and downwelling sheets found in small domains, illustrating the importance of simulating wide domains. The addition of depth dependence results in small cells and reverses the planform, causing hot plumes and cold sheets. The planform of temperature dependent viscosity convection is due predominantly to vertical variations in viscosity resulting from the temperature dependence. Compressibility, with associated depth-dependent properties, results in a tendency for broad upwelling plumes and narrow downwelling sheets, with large aspect ratio cells. Perhaps the greatest modulation effect occurs in internally heated compressible cases, in which the short-wavelength pattern of time-dependent cold plumes commonly observed in constant-viscosity calculations completely changes into a very long wavelength pattern of downwelling sheets (spaced up to 24,000 km apart) with time-dependent plumelike instabilities. These results are particularly interesting, since the basal heat flow in the Earth's mantle is usually thought to be very low, e.g., 5-20% of total. The effects of viscous dissipation and adiabatic heating play only a minor role in the overall heat budget for constant-viscosity cases, an observation which is not much affected by the Rayleigh number. However, viscous dissipation becomes important in the stiff upper boundary layer when viscosity is temperature dependent. This effect is caused by the very high stresses occurring in this stiff lid, typically 2 orders of magnitude higher than the stresses in the interior of the domain for the viscosity contrast modeled here. The temperature in the interior of convective cells is highly sensitive to the material properties, with temperature dependent viscosity and depth-dependent thermal conductivity strongly increasing the internal temperature, and depth-dependent viscosity strongly decreasing it. The sensitivity of the observed flow pattern to these various complexities clearly illustrates the importance of performing compressible,

Abstract. A systematic investigation into the effects of temperature dependent viscosity on three-dimensional compressible mantle convection has been performed by means of numerical simulations in Cartesian geometry using a finite volume multigrid code, with a factor of 1000-2500 viscosity variation, Rayleigh numbers ranging from 10^5-10^7, and stress-free upper and lower boundaries. Considerable differences in model behavior are found depending on the details of rheology, heating mode, compressibility, and boundary conditions. Parameter choices were guided by realistic Earth models. In Boussinesq, basally heated cases with viscosity solely dependent on temperature and stress-free, isothermal boundaries, very long wavelength flows (~25,000 km, assuming the depth corresponds to mantle thickness) with cold plumes and hot upwelling sheets result, in contrast to the upwelling plumes and downwelling sheets found in small domains, illustrating the importance of simulating wide domains. The addition of depth dependence results in small cells and reverses the planform, causing hot plumes and cold sheets. The planform of temperature dependent viscosity convection is due predominantly to vertical variations in viscosity resulting from the temperature dependence. Compressibility, with associated depth-dependent properties, results in a tendency for broad upwelling plumes and narrow downwelling sheets, with large aspect ratio cells. Perhaps the greatest modulation effect occurs in internally heated compressible cases, in which the short-wavelength pattern of time-dependent cold plumes commonly observed in constant-viscosity calculations completely changes into a very long wavelength pattern of downwelling sheets (spaced up to 24,000 km apart) with time-dependent plumelike instabilities. These results are particularly interesting, since the basal heat flow in the Earth's mantle is usually thought to be very low, e.g., 5-20% of total. The effects of viscous dissipation and adiabatic heating play only a minor role in the overall heat budget for constant-viscosity cases, an observation which is not much affected by the Rayleigh number. However, viscous dissipation becomes important in the stiff upper boundary layer when viscosity is temperature dependent. This effect is caused by the very high stresses occurring in this stiff lid, typically 2 orders of magnitude higher than the stresses in the interior of the domain for the viscosity contrast modeled here. The temperature in the interior of convective cells is highly sensitive to the material properties, with temperature dependent viscosity and depth-dependent thermal conductivity strongly increasing the internal temperature, and depth-dependent viscosity strongly decreasing it. The sensitivity of the observed flow pattern to these various complexities clearly illustrates the importance of performing compressible, variable-viscosity mantle convection calculations with rheological and thermodynamic properties matching as closely as possible those of the Earth.

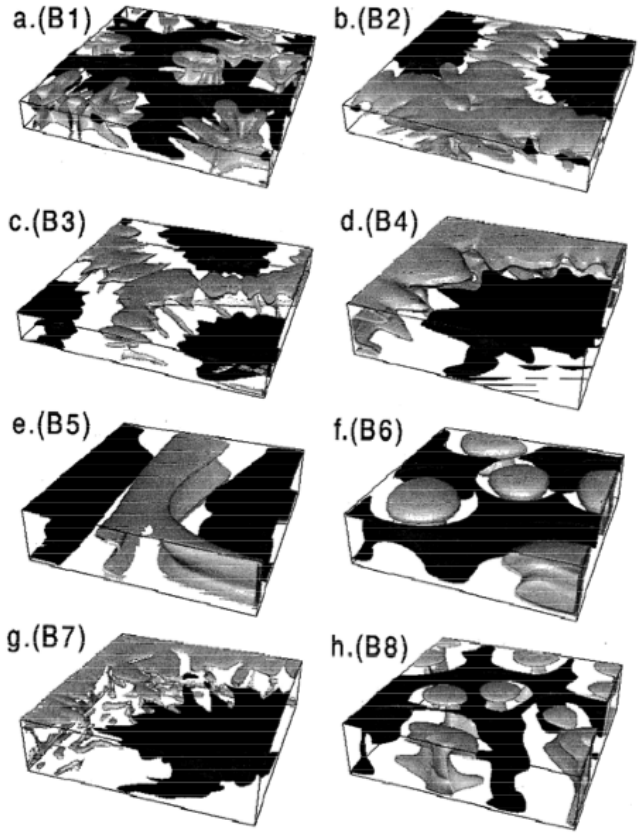

Figure 2. Convective patterns for Boussinesq, basally heated cases. Plotted are isosurfaces of residual temperature (i.e., temperature relative to horizontally averaged value). Light contours indicate upwellings, showing where the temperature is 0.1 hotter than the horizontal average; dark contours indicate downwellings, showing where the temperature is 0.1 colder than the horizontal average. (a) Constant viscosity, Ra=10^5 (B1); (b) $\eta(T)$, periodic sides, Ra=10^5 (B2); (c) $\eta(T)$, reflecting sides, Ra=10^5 (B3); (d) $\eta(T)$, aspect ratio 4, Ra=10^5 (B4), displaying the same solution as B2; (e) $\eta(Z)$, Ra=10^5 (B5); (f) $\eta(T,Z)$, Ra=10^5 (B6); (g) $\eta(T)$, Ra=10^6 (B7); and (h) $\eta(T,Z)$, Ra=10^6 (B8). For further details, see Table 2.

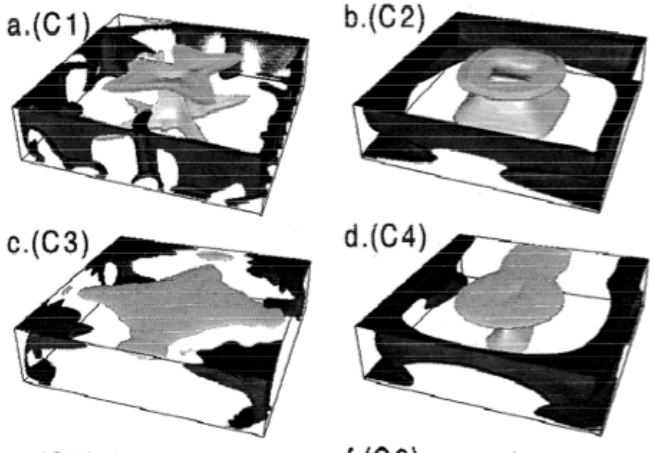

Conclusions

These results show that a considerable range of convective styles and characteristic horizontal wavelengths is possible, depending on the exact details of rheology, compressibility, heating mode, and Rayleigh number. All of these have a significant effect on the flow, indicating the importance of including them into numerical models, and matching the Earth's parameter space as closely as possible.

Results obtained under the Boussinesq approximation show clearly the importance of modeling wide domains. With rheology being dependent solely on temperature and stress-free boundaries, very wide cells are formed (periodicity 8) with upwelling sheets and downwelling plumes, in contrast to the small-wavelength spoke pattern obtained with rigid boundaries [*White*, 1988; *Tackley*, 1993]. *Christensen and Harder* [1991] previously concluded that upwelling sheets are unlikely to occur in temperature dependent viscosity convection. However, these results indicate that at sufficiently large aspect ratio and with stress-free boundaries, they are the preferred solution. Adding depth dependence completely reverses these characteristics, resulting in small cells with upwelling plumes and downwelling sheets. Increasing the Rayleigh number by an order of magnitude does not appear to fundamentally change the convective pattern, resulting in narrower features and greater time dependence, and in some cases, smaller cell sizes. To first order, changes in planform arising from temperature dependent viscosity are due mainly to the mean depth dependence introduced by temperature dependence.

Compressibility, with the associated depth-dependent material properties, results in fairly large cells for basally heated models, and a preference for large upwelling plumes and narrow downwelling sheets. However, when the viscosity is dependent solely on temperature, downwelling plumes and linear upwellings are observed, in accordance with the equivalent Boussinesq solutions.

Perhaps the greatest modulation effect of viscosity variations occurs in internally heated, compressible cases. It is through a self-regulation mechanism first described by *Tozer* [1972], and thus the effect of various parameters on the internal mantle temperature may be lower than that predicted by these simulations. The interior temperature profile (away from boundary layers) is always close to adiabatic, and usually somewhat subadiabatic.

The convective vigor, as measured by rms velocity, is diminished in regions of high viscosity. However, in these calculations, the stiff upper boundary layer still participates in the flow; a larger viscosity contrast would be necessary to cause a rigid lid. The stress distribution resembles the viscosity distribution, with very high stress levels in the upper boundary layer.

Examination of the energy balance reveals that viscous dissipation and adiabatic heating are only minor contributors to the heat budget for constant-viscosity compressible mantle convection, with advection and diffusion playing the dominant role. Although the magnitude of viscous dissipation and adiabatic heating terms increases with Rayleigh number, advection and diffusion terms increase by a similar or larger factor, and thus viscous dissipation and adiabatic heating are still relatively unimportant. However, when temperature dependent viscosity is included, viscous dissipation becomes important in the stiff upper boundary layer due to the high stresses.

In these results, realistic plates and subduction are not obtained. Temperature dependent viscosity by itself does not result in plate-like behavior. The downwellings are two-sided, and a concentration of stress occurs where they leave the upper boundary layer. In order for plates to occur, an additional mechanism is needed to create weak zones in the stiff lid, such as nonlinear powerlaw rheology [*Cserepes*, 1982; *Christensen*, 1984; *Weinstein and Olson,* 1992], or a "stick-slip" rheology [*Bercovici*, 1993, 1995]. A priority in future work must be to examine the influences of these rheologies in self-consistent three-dimensional models. Other priorities include the effects of phase transitions, spherical geometry, compositional variations, and continents. Other possible rheological complexities not considered here include

Earth and Planetary Science Letters 401 (2014) 172–182

Contents lists available at ScienceDirect

Earth and Planetary Science Letters

www.elsevier.com/locate/epsl

The effect of plate motion history on the longevity of deep mantle heterogeneities

Abigail L. Bull [a,*], Mathew Domeier [a], Trond H. Torsvik [a,b,c]

[a] Centre for Earth Evolution and Dynamics (CEED), University of Oslo, 0316 Oslo, Norway
[b] Geodynamics, Geological Survey of Norway, 7491 Trondheim, Norway
[c] School of Geosciences, Witwatersrand University, WITS 2050 Johannesburg, South Africa

$$\nabla \cdot u = 0$$

where u is the velocity vector. The momentum equation is

$$-\nabla P + \nabla \cdot (\eta \dot{\varepsilon}) = (RaT - Rbc)\hat{\boldsymbol{r}}$$

where $\hat{\boldsymbol{r}}$ is the radial unit vector, P is the dynamic pressure, η is the viscosity, ε is the strain rate tensor, T is the temperature, c is the composition and Ra is the thermal Raleigh number defined as

$$Ra = \frac{\alpha \rho g \Delta T h^3}{\eta \kappa}$$

where α is the thermal expansivity, ρ is the density, g is the acceleration due to gravity, ΔT is the temperature drop across the mantle, h is the mantle thickness and κ is the thermal diffusivity. We employ a Rayleigh number of 2×10^8.

The chemical Rayleigh number, Rb, is defined as

$$Rb = \frac{\Delta \rho g h^3}{\eta \kappa}$$

where $\Delta\rho$ is the density contrast between chemical components. The buoyancy ratio, B, which is the ratio of chemical to thermal buoyancy is defined as

$$B = \frac{Rb}{Ra} = \frac{\Delta \rho}{\rho \alpha \Delta T}$$

The energy equation is defined as

$$\frac{\partial T}{\partial t} + (\boldsymbol{u} \cdot \nabla) T = \nabla^2 T + H$$

where t is time and H is the non-dimensional internal heating rate.

We employ a temperature- and depth-dependent rheology of the non-dimensional form:

$$\eta(T, \vec{z}) = \eta_r(z) \exp\left[A(0.5 - T)\right]$$

where $\eta_r(z) = 1$ for $z < 663$ km and $\eta_r(z) = 0.1225z - 51.2$ for 663 km $\leq z \leq$ 2867 km. η and z are the non-dimensional viscosity and dimensional depth respectively. This is similar to the viscosity structure used in McNamara and Zhong (2005), Bull et al. (2009) and Zhang et al. (2010) and leads to a weak upper mantle, a 30× viscosity step at the boundary between the upper and lower mantle, and a 10× linear increase with depth to the base of the mantle. The non-dimensional activation coefficient is chosen

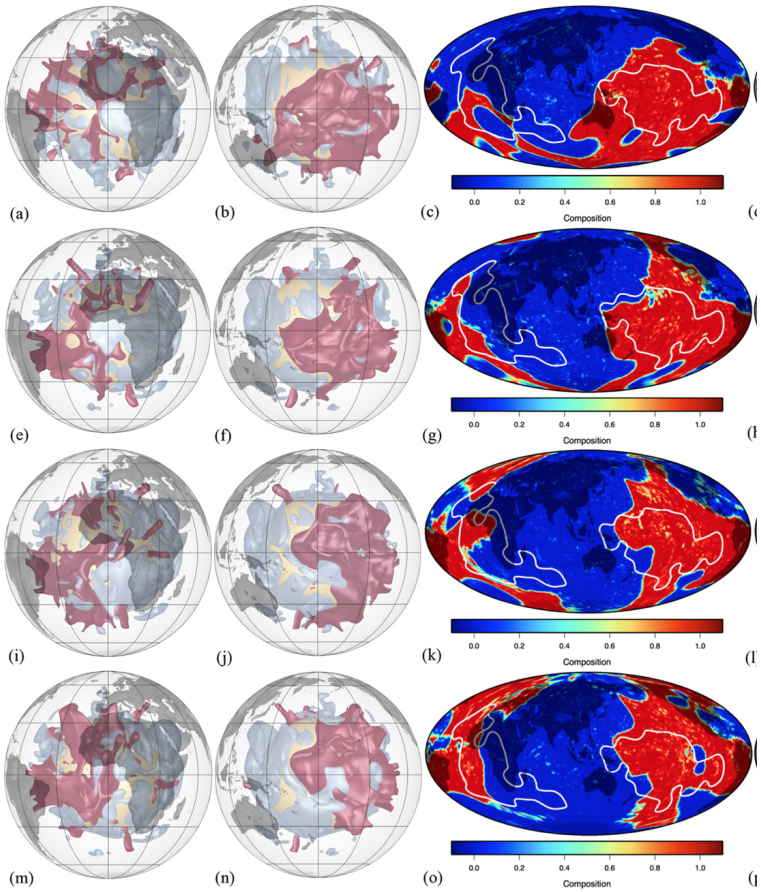

Geochemistry Geophysics Geosystems G3
AN ELECTRONIC JOURNAL OF THE EARTH SCIENCES
Published by AGU and the Geochemical Society

Article
Volume 10, Number 1
28 January 2009
Q01006, doi:10.1029/2008GC002151
ISSN: 1525-2027

Effect of mantle compressibility on the thermal and flow structures of the subduction zones

Changyeol Lee and Scott D. King
Department of Geosciences, Virginia Polytechnic Institute and State University, 4044 Derring Hall, Blacksburg, Virginia 24061, USA (cylee@vt.edu)

[1] The heat generated by viscous dissipation is consistently evaluated using a 2-D compressible subduction model with variations of mantle rheology (constant as well as pressure and temperature dependent viscosity), dip, age, and velocity of the subducting slab. For comparison, we also conduct 2-D incompressible subduction calculations with the same conditions and parameters used in the compressible formulation. The effect of compressibility on the thermal and flow structures of the subduction zones is relatively small and concentrated along the base of the mantle wedge, with temperature differences <100°C and differences in kinematic energy of the mantle wedge <1% between compressible and incompressible models. Mantle rheology has a stronger effect on thermal and flow structures than mantle compressibility as well as the variations of dip, age, and velocity of the subducting slab. The heat from viscous dissipation in the compressible model increases the slab temperatures over the incompressible model (<70°C), as a result of additional conduction across the slab surface (constant viscosity) and thinning of the thermal boundary layer caused by viscosity reduction (pressure- and temperature-dependent viscosity).

Components: 13,868 words, 15 figures, 2 tables.

Keywords: subduction zone; compressible model; viscous dissipation.

Index Terms: 4255 Oceanography: General: Numerical modeling (0545, 0560); 8170 Tectonophysics: Subduction zone processes (1031, 3060, 3613, 8413).

Received 2 July 2008; **Revised** 31 October 2008; **Accepted** 25 November 2008; **Published** 28 January 2009.

Lee, C., and S. D. King (2009), Effect of mantle compressibility on the thermal and flow structures of the subduction zones, *Geochem. Geophys. Geosyst.*, *10*, Q01006, doi:10.1029/2008GC002151.

1. Introduction

[2] Subduction zones are the sites where active arc volcanoes, orogenic processes, and destructive earthquakes from shallow to deep are observed. The mantle wedge between the slab and overlying lithosphere is expected to be cooler than that of the ambient upper mantle due to a cold subducting slab. However, both geochemistry of arc magmas and surface heat flow data in the arc and backarc seem to require high temperatures in the mantle wedge [*Currie et al.*, 2004; *Currie and Hyndman*, 2006; *Furukawa and Uyeda*, 1989; *Kelemen et al.*, 2003; *Peacock and Hyndman*, 1999; *Peacock*, 2003; *Peacock et al.*, 2005; *Ulmer*, 2001]. To reconcile these seemingly contradictory observations, previous studies have suggested induced hot mantle from deep mantle to the corner of the mantle wedge by viscous coupling between the subducting slab and mantle wedge or small-scale mantle convection below the backarc [*Currie et al.*, 2004; *Kelemen et al.*, 2003; *Peacock et al.*, 2005; *van Keken et al.*, 2002]. Although the heat gener-

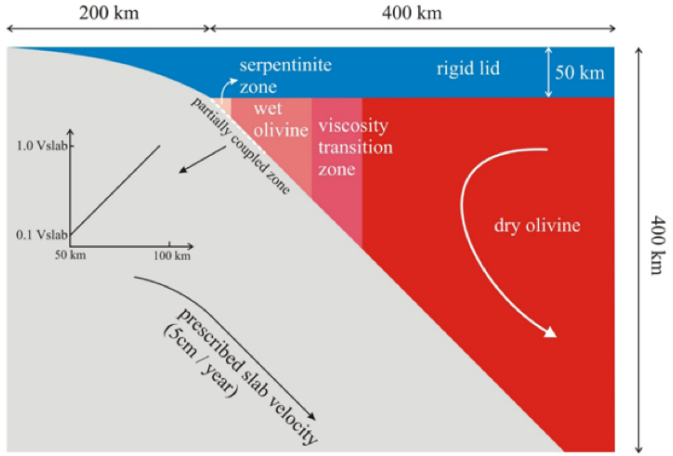

Figure 1. Schematic diagram of the subduction zone model using the dip of 45 degrees for the straight slab and the subducting slab velocity of 5 cm/a. The subducting slab and upper mantle below the slab are subducted together. For details about initial and boundary conditions, rheology, and a decoupling condition, see text.

[12] In this study, we formulate a 2-D numerical subduction model consisting of a prescribed subducting slab, a 50 km thick overlying rigid lid (lithosphere) and the mantle wedge between the slab and lid (Figure 1). Because the main purpose of this study is to evaluate the effect of the mantle compressibility on the thermal and flow structures of the subduction zones, geometry of the subduction model here is arbitrary and simplified. Similar numerical models have been used in previous studies [e.g., *Currie et al.*, 2004; *Davies and*

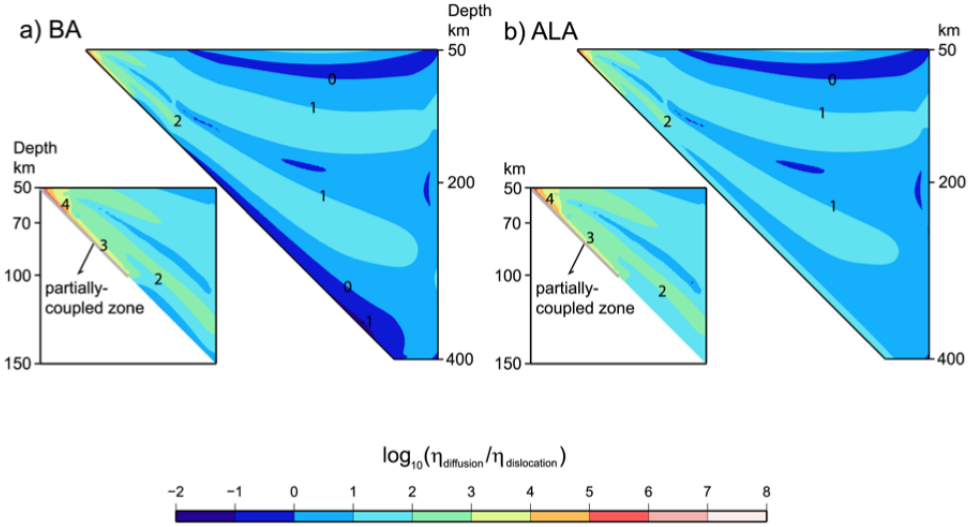

Figure 7. Log-scaled viscosity ratio of diffusion to dislocation creep in the mantle wedge for the (a) BA and (b) ALA experiments using composite viscosity. Dislocation creep becomes the predominant mantle rheology in the region where strain rate is high, especially, by the partially coupled zone. In the ALA experiments using composite viscosity (Figure 7b), the predominance of dislocation creep above the slab surface is extended to the bottom of the box.

5. Conclusion

[40] We conduct numerical subduction experiments using incompressible (BA) and compressible (ALA) fluid models to evaluate the effect of compressibility on the thermal and flow structures of the subduction zones. Variations of dip, age, and velocity of the subducting slab are considered with constant viscosity and pressure- and temperature-dependent viscosity. In general, there are only small differences between the results from the BA and ALA experiments. Unlike compressibility, rheology is a more important factor affecting the thermal and flow structures of the subduction zones; we observe lower surface heat flow in the arc in the BA and ALA experiments using constant viscosity and higher surface heat flow, faster slab heating, and a very thick thermal lithosphere below the backarc in the BA and ALA experiments using pressure- and temperature-dependent viscosity. We find that compressibility affects the slab temperature through a feed back with the heat generated by viscous dissipation. In the ALA experiments using constant viscosity, the heat generated by viscous dissipation increases the slab temperature faster

Physics of the Earth and Planetary Interiors 216 (2013) 74–90

Contents lists available at SciVerse ScienceDirect

Physics of the Earth and Planetary Interiors

journal homepage: www.elsevier.com/locate/pepi

Geoid and topography of Earth-like planets: A comparison between compressible and incompressible models for different rheologies

Meysam Shahraki *, Harro Schmeling

Faculty of Earth Sciences, Section Geophysics, Room 1.226, J.W. Goethe University, Altenhöferallee 1, 60438 Frankfurt M, Germany

ARTICLE INFO

Article history:
Received 12 May 2012
Received in revised form 13 November 2012
Accepted 31 December 2012
Available online 10 January 2013
Edited by Mark Jellinek

Keywords:
Earth-like planets
Geoid anomaly
Dynamic topography
Compressible
Arrhenius rheology

ABSTRACT

A systematic study of 2D-axisymmetric, spherical shell models of compressible and incompressible mantle convection with constant and variable viscosity and constant and depth-dependent thermodynamic properties is presented. To account for compressibility effects, we employ the anelastic liquid approximation. In the case of variable viscosity, an Arrhenius law with strongly temperature and pressure dependent viscosity is considered. We show that assuming compressible convection with depth-dependent thermodynamic properties strongly influence the geoid undulations. Using compressible convection with constant thermodynamic properties is physically inconsistent and may lead to spurious results for the geoid and convection pattern. In addition, we examine the impact of compressibility as well as different rheologies on the power law relation that connects the Nusselt number to the Rayleigh number. We discover that the power law index of the Nu–Ra relationship is controlled by the rheology, independent of which approximation is used. Instead, the bound of this relation is controlled by a combination of different approximation and rheology.

1. Introduction

Since almost five decades mantle convection has been studied by numerical models. Because of the limitations imposed by finite computing capacity, several simplifying assumptions have commonly been made in most mantle convection studies. One of the most important of such assumptions is the Boussinesq approximation. This approximation is valid if the temperature scale height (i.e. the depth over which temperature increases by a factor of "e" due to adiabatic compression) is much greater than the convection depth (Mihaljan, 1962; Spiegel and Veronis, 1960). However, a temperature scale height in the Earth's mantle is at best only slightly greater than the mantle depth. Hence, the Boussinesq approximation could mask some very important stratification and compressibility effects that influence both the spatial and temporal structure of the convection (Glatzmaier, 1988).

Since the whole mantle thickness of Venus, Earth and Mars are between 45% and 50% of mean planetary radius (Stevenson et al., 1983), global models of mantle convection require a spherical geometry (Bercovici et al., 1992). The pioneer series study of mantle convection in spherical geometry has been done by Zebib (e.g. Zebib et al., 1985; Zebib and Schubert, 1979; Zebib et al., 1983; Zebib et al., 1978, 1980). Following these studies, a number of other studies in spherical geometry focusing on effects such as phase changes, variable viscosity, etc. have been published (see e.g. Schubert et al. (2001) for more references). However, in almost all early models the Boussinesq approximation has been used to simplify the equations governing fluid motion in order to facilitate numerical computation. Different challenges can be encountered if one is interested in the geoid, because the density is the primary variable for the geoid. Therefore, it is important to go beyond the Boussinesq approximation for the geoid computation.

Indeed, the importance of compressible convection has been discovered in two-dimensional Cartesian geometry for iso-viscous convection (Jarvis and McKenzie, 1980) and for variable viscosity (Quareni et al., 1986; Yuen et al., 1987), without looking at the geoid except for a study by Schmeling (1989) who investigated the geoid variation in two-dimensional variable viscosity compressible convection. However, Cartesian geoid is not helpful if to be compared to the real Earth, and spherical models are necessary. Moreover, he computed the geoid undulations by neglecting depth-dependence of the thermodynamic parameters, although the variations of the bulk modulus, thermal expansion and thermal conductivity are known to be large across the Earth's mantle (e.g. Anderson, 1987).

Recently, three-dimensional compressible convection with depth-dependent thermodynamic properties attracted great attention (e.g. Tackley, 1996, 2008). Yet, such studies did not focus on the geoid for compressible cases, especially with depth-dependent properties.

* Corresponding author. Tel.: +46 (0)69 79840115; fax: +46 (0)69 79840131.
E-mail addresses: shahraki@geophysik.uni-frankfurt.de, meysam.shahraki@gmail.com (M. Shahraki).

1. Introduction

Since almost five decades mantle convection has been studied by numerical models. Because of the limitations imposed by finite computing capacity, several simplifying assumptions have commonly been made in most mantle convection studies. One of the most important of such assumptions is the Boussinesq approximation. This approximation is valid if the temperature scale height (i.e. the depth over which temperature increases by a factor of "e" due to adiabatic compression) is much greater than the convection depth (Mihaljan, 1962; Spiegel and Veronis, 1960). However, a temperature scale height in the Earth's mantle is at best only slightly greater than the mantle depth. Hence, the Boussinesq approximation could mask some very important stratification and compressibility effects that influence both the spatial and temporal structure of the convection (Glatzmaier, 1988).

Since the whole mantle thickness of Venus, Earth and Mars are between 45% and 50% of mean planetary radius (Stevenson et al., 1983), global models of mantle convection require a spherical geometry (Bercovici et al., 1992). The pioneer series study of mantle convection in spherical geometry has been done by Zebib (e.g. Zebib et al., 1985; Zebib and Schubert, 1979; Zebib et al., 1983; Zebib et al., 1978, 1980). Following these studies, a number of other studies in spherical geometry focusing on effects such as phase changes, variable viscosity, etc. have been published (see e.g. Schubert et al. (2001) for more references). However, in almost all early models the Boussinesq approximation has been used to simplify the equations governing fluid motion in order to facilitate numerical computation. Different challenges can be encountered if one is interested in the geoid, because the density is the primary variable for the geoid. Therefore, it is important to go beyond the Boussinesq approximation for the geoid computation.

Indeed, the importance of compressible convection has been discovered in two-dimensional Cartesian geometry for iso-viscous convection (Jarvis and McKenzie, 1980) and for variable viscosity (Quareni et al., 1986; Yuen et al., 1987), without looking at the geoid except for a study by Schmeling (1989) who investigated the geoid variation in two-dimensional variable viscosity compressible convection. However, Cartesian geoid is not helpful if to be compared to the real Earth, and spherical models are necessary. Moreover, he computed the geoid undulations by neglecting depth-dependence of the thermodynamic parameters, although the variations of the bulk modulus, thermal expansion and thermal conductivity are known to be large across the Earth's mantle (e.g. Anderson, 1987).

Recently, three-dimensional compressible convection with depth-dependent thermodynamic properties attracted great attention (e.g. Tackley, 1996, 2008). Yet, such studies did not focus on

2.1. Reference state

The reference state is that of an adiabatic, homogenous fluid under hydrostatic pressure. In this reference state the density distribution, ρ_r, can be obtained as the solution of the Adams-Williamson equation,

$$\frac{1}{\rho_r}\frac{d\rho_r}{dr} = -\frac{\rho_r g}{K_{ad}} = -\frac{\alpha g}{c_p \gamma} \tag{8}$$

where K_{ad} is the adiabatic incompressibility and, γ is the Grüneisen parameter which is a measure of the anharmonic character of the equation of the state (Balachandar et al., 1993) defined as:

$$\gamma = \frac{\alpha K_{ad}}{\rho_r c_p}. \tag{9}$$

According to the condition of $\frac{\alpha}{\gamma} \propto \rho^{-2}$ (Leitch et al., 1992), Zhang and Yuen (1996) simplified this equation and derived:

$$\rho_r = \rho_0 \left[1 + \frac{2D_{i0}}{\gamma_0}\frac{(r_0 - r)}{d}\right]^{1/2} \tag{10}$$

where $D_{i0} = \alpha_0 g d/c_p$ is the surface dissipation number and r_0, ρ_0 are outer radius of the shell and density at the top surface, respectively (see Table 1).

The pressure and temperature-dependence of the thermal conductivity (for mantle materials) is not well understood. However, in the first order of a theoretical estimation of Anderson (1987) based on lattice dynamics, we considered a thermal conductivity, which varies with depth according to

$$k = k_0 \left(\frac{\rho_r}{\rho_0} \right)^3, \tag{11}$$

in which k_0 is the surface value of the thermal conductivity (see Table 1).

This equation implies an increase of k by a factor of 2.5 to the core mantle boundary (CMB) (see Fig. 1). Recently several experimental and theoretical simulations have been conducted which suggest a strong variation in k (e.g. Hofmeister, 2008). However, no conclusive agreement has been reached. Therefore, we consider the first order of approximation in our simulations. In addition, the gravitational acceleration, g, is taken to be constant, since the acceleration due to gravity does not differ from 10.1 ms^{-2} by more than 6% throughout the entire mantle (Dziewonski and Anderson, 1981). Besides, Q, the internal heating rate is also assumed to be zero. Of course, radioactive sources in the mantle contribute to the heat production over a period of Myrs, and this heating rate undoubtedly varies with time, but for the purposes of present study, it is an additional complexity that would be distracting; therefore, it will be neglected.

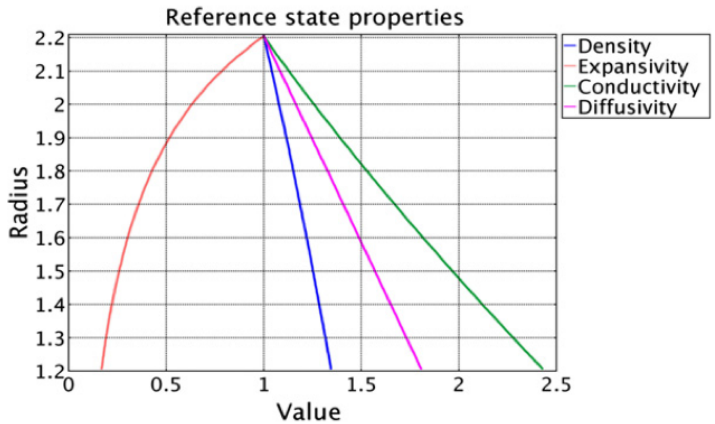

Fig. 1. Variation of dimensionless reference state with parameters value listed in Table 1 The non-dimensional x-axis is density (blue), thermal expansion (red), thermal conductivity (green) and diffusivity (magenta) with non-dimensional radius on y-axis. (For interpretation of the references to color in this figure legend, the reader is referred to the web version of this article.)

We consider the thermal expansivity decreasing with increasing density (Chopelas and Boehler, 1992) according to

$$\alpha = \alpha_0 \left(\frac{\rho_r}{\rho_0} \right)^{-6}. \tag{12}$$

This implies a decrease in thermal expansion by a factor of five from the top to the CMB (Fig. 1). We neglect the temperature dependence of thermal expansivity, although it may be important for heat transport and velocities in the upper mantle (Ghias and Jarvis, 2008; Schmeling et al., 2003).

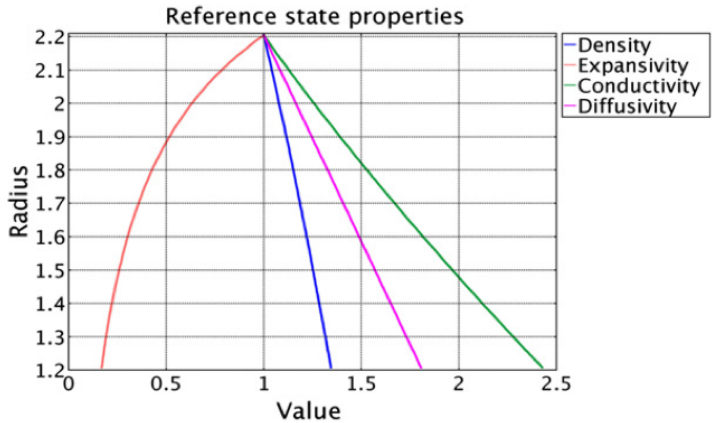

Fig. 1. Variation of dimensionless reference state with parameters value listed in Table 1 The non-dimensional *x*-axis is density (blue), thermal expansion (red), thermal conductivity (green) and diffusivity (magenta) with non-dimensional radius on *y*-axis. (For interpretation of the references to color in this figure legend, the reader is referred to the web version of this article.)

However, if we aim to obtain a complete understanding of the mantle convection process, viscosity variations are essential components which have to be taken with care. Therefore, we attempt to get close to a realistic temperature–pressure-dependent viscosity by taking the Arrhenius law according to the new formulation introduced by Shahraki and Schmeling (2012), in which they have tried to adjust the activation energy, E, the activation volume, V_a, and pre-exponential constant, A, by taking them as unknowns in a system of equations and then use these values in the Newtonian viscosity as known constants.

$$\eta = A \exp\left(\frac{E + Bz}{R_g T}\right) \tag{13}$$

Here, T is the absolute temperature and z is the depth. In addition, R is the gas constant and B is an abbreviation which is equal to $B = \rho g V_a$, where ρ and g are the density and the gravity acceleration, respectively.

It should be noted that, in general, our viscosity profiles are in agreement with viscosity profiles based on observations and inversions (e.g. Steinberger and Calderwood, 2006). This means that there is a highly viscous layer at the top surface underlain by a layer whose viscosity decreases considerably towards the 660 discontinuity (Fig. 2). Below, the viscosity increases towards the CMB so that there is a hump in the lower mantle which has been inferred in previous studies of geoid and post-glacial rebound inversions (e.g. Forte and Mitrovica, 2001; Mitrovica and Forte, 2004; Ricard and Wuming, 1991; Soldati et al., 2009). Furthermore, in

The main purpose of this work is to point out the differences between two different common approximations in the geodynamic community. The first group of the models is incompressible with the Extended Boussinesq approximation (EB), and the second group is compressible with the Anelastic Liquid Approximation assuming depth-dependent thermodynamics properties (CM). However, to better analyze those two approximations and to analyze which behavior stems from compressibility and which from the depth dependence of the other parameters, a third group is also taken into consideration to show its validity with respect to what we presume are the more realistic or consistent approaches (EB and CM). Basically, this group is the same as the second group, except that the thermodynamic properties are assumed to be constant (CMC).

In our view, the CMC group is not fully thermodynamically consistent because on one hand compression is allowed to generate depth dependent density, but on the other hand, these density variations are not allowed to generate appropriate variations in other thermodynamic properties such as thermal expansivity or conductivity. Thus, using compressible formulations with depth-dependent density implicitly requires also thermodynamic properties be depth-dependent. Therefore, modeling compressible approaches with constant thermodynamic properties are, strictly speaking, physically inconsistent. Here we include one set of models with this inconsistent assumption to explore the consequences.

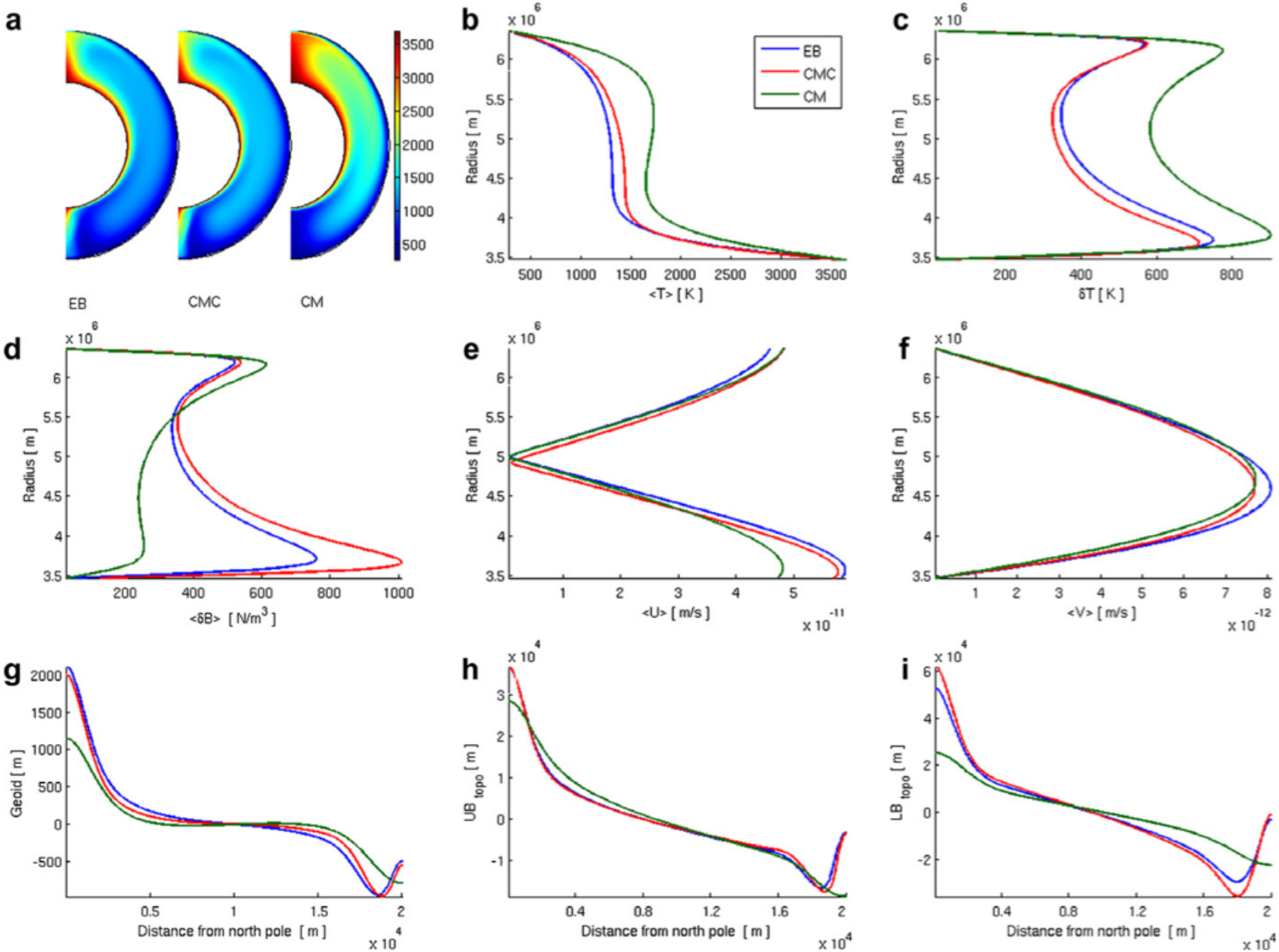

Fig. 3. Convection models with iso-viscous viscosity. (a) Temperature distributions of three different configuration; (b) profiles of the spherically averaged temperature; (c) RMS residual temperature; (d) RMS-buoyancy; (e) spherically averaged of the absolute horizontal velocity; (f) spherically avenged of the absolute vertical velocity; (g) geoid undulation; (h) surface dynamic topography; (i) core–mantle-boundary topography. The blue, red and green profiles correspond to the EB, CMC and CM models respectively. (For interpretation of the references to color in this figure legend, the reader is referred to the web version of this article.)

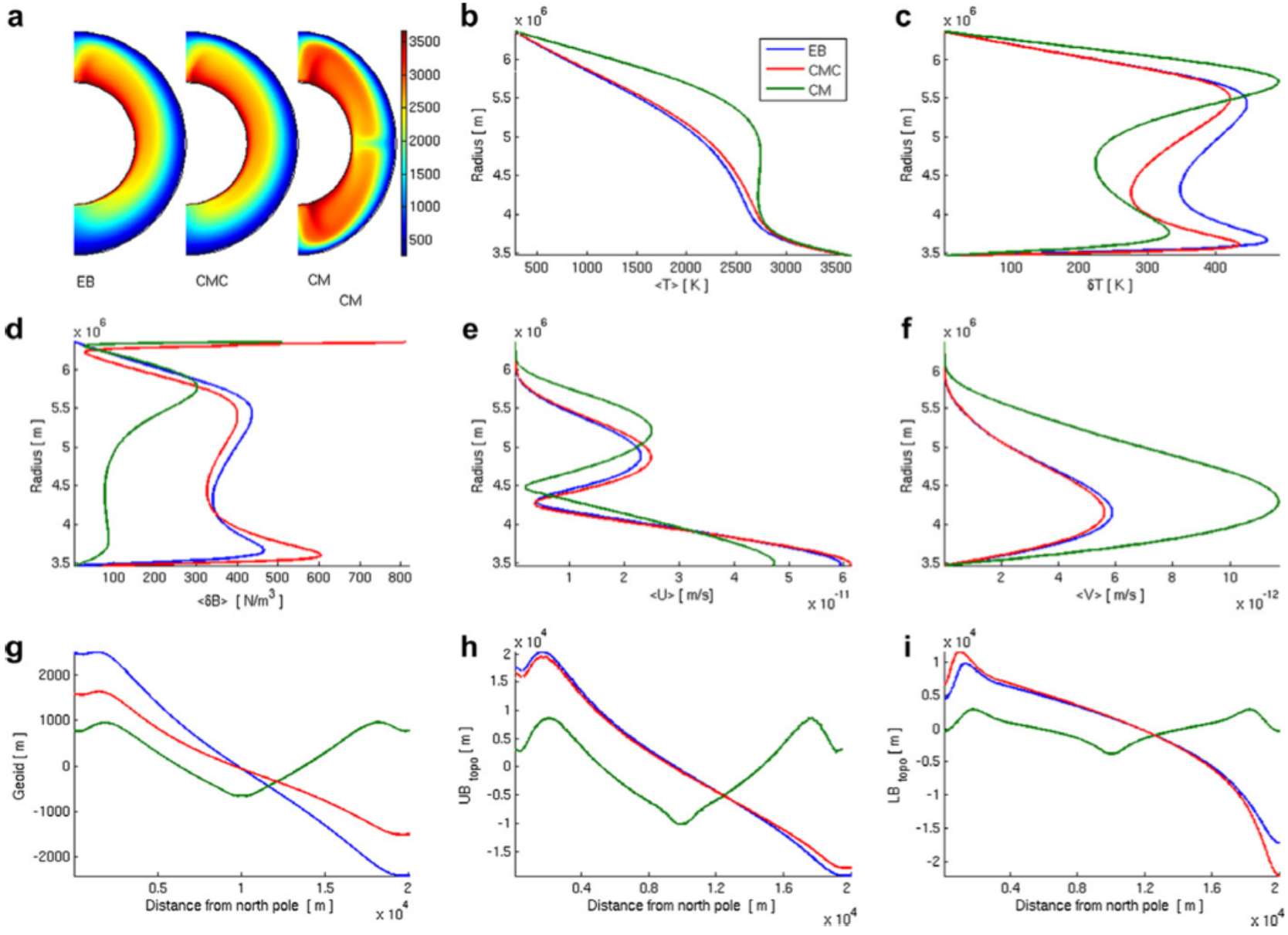

Fig. 4. Same as Fig. 3, but for convection models with temperature-dependent viscosity.

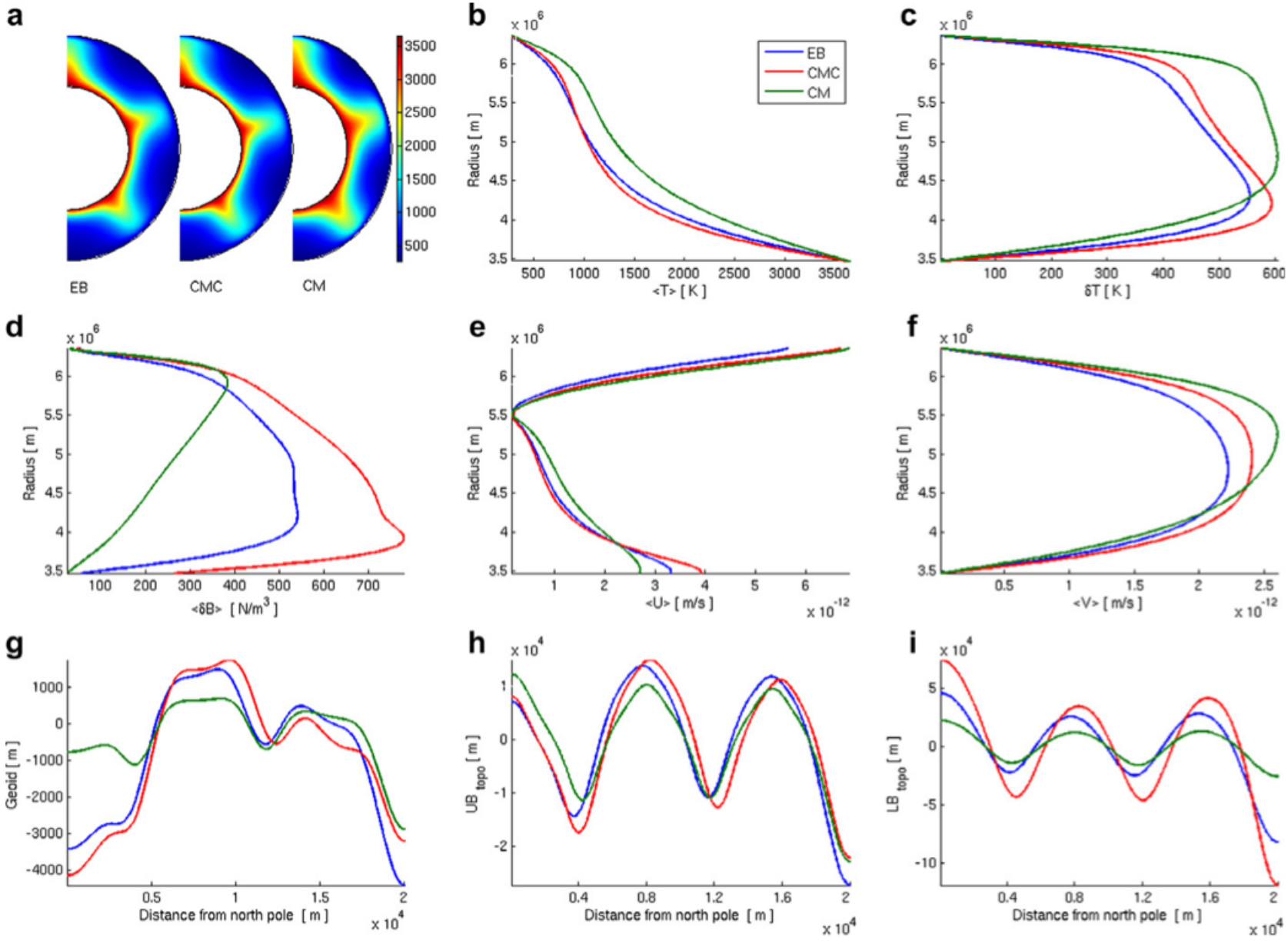

Fig. 5. Same as Fig. 3, but for convection models with pressure-dependent viscosity.

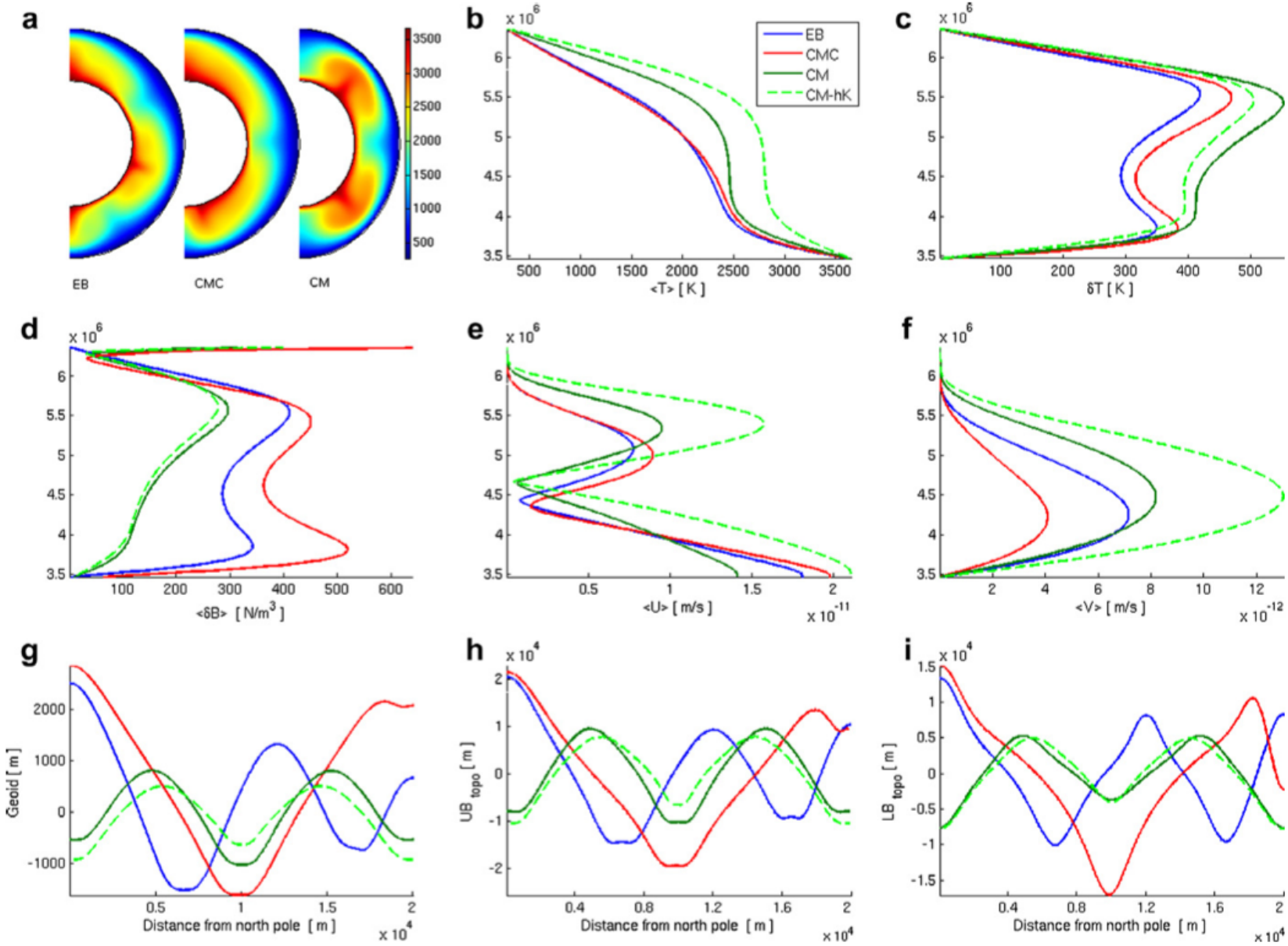

Fig. 6. Same as Fig. 3, but for convection models with temperature and pressure-dependent viscosity. Dashed green curves are corresponding to the compressible convection model in which the thermal conductivity increases strongly with depth. (For interpretation of the references to color in this figure legend, the reader is referred to the web version of this article.)

5. Conclusion

(a) A systematic study comparing different approaches of compressibility in the spherical shell axi-symmetric convection for different Arrhenius viscosity laws shows that only in the unrealistic case of zero activation energy the different compressibility modes result in comparable convection and geoid patterns. In all other rheological cases, large differences have been obtained, stressing the important role of consistent compressible thermodynamic properties for mantle convection.

(b) When considering compressible convection in the Earth-like planets it is essential not only to include variable density but also the density dependence of other thermodynamic properties. Considering only variable density may lead to inconsistent results for the geoid and dynamic topography as well as the convection pattern.

(c) The indirect effect of variable density on thermodynamic properties is more important in modifying spherical shell convection and geoid than the variable density alone.

(d) Compared to the EB and ALA models with no depth-dependent thermodynamic parameters fully compressible convection seems to avoid rising plumes at the poles in axi-symmetric convection.

(e) As the Rayleigh number increases from the first critical value to the second critical value (representing the transition to time dependent convection), in the case of the temperature–pressure-dependent viscosity, the Nu–Ra relationship is strongly dependent on the aspect ratio of the convection cell while in the iso-viscous case, a weak dependence observed.

(f) The efficiency of the Arrhenius temperature-dependent viscosity as well as temperature–pressure-dependent viscosity in the mantle to remove the heat is weakly dependent on the Ra number, and it is almost independent of using different compressibility approximations.

AGU PUBLICATIONS

JGR

Journal of Geophysical Research: Solid Earth

RESEARCH ARTICLE

10.1002/2014JB011150

Key Points:
- Three-dimensional numerical modeling of western Mediterranean subduction evolution since 35 Ma
- Modeled subduction evolution distinguishes between disparate tectonic scenarios
- Preferred model matches observed

Underpinning tectonic reconstructions of the western Mediterranean region with dynamic slab evolution from 3-D numerical modeling

M. V. Chertova[1], W. Spakman[1,2], T. Geenen[3], A. P. van den Berg[1], and D. J. J. van Hinsbergen[1]

[1]Department of Earth Sciences, Utrecht University, Utrecht, Netherlands, [2]Centre of Earth Evolution and Dynamics, University of Oslo, Oslo, Norway, [3]SURFsara, Amsterdam, Netherlands

We model the evolution of the western Mediterranean region with the finite element modeling package SEPRAN (http://ta.twi.tudelft.nl/sepran/sepran.html). We solve the following three dimensionless equations (used symbols are given in Table 1) applying the extended Boussinesq approximation for a medium including solid state phase transitions [*Christensen and Yuen*, 1984]:

Mass conservation of an incompressible viscous fluid,

$$\partial_j v_j = 0, \tag{1}$$

the Stokes equation describing force balance,

$$-\partial_i P + \partial_j \tau_{ij} = \left(RaT - \sum\nolimits_k Rb_k \Gamma_k\right) g_i, \tag{2}$$

and the heat conservation equation:

$$\frac{\partial T}{\partial t} + v_j \partial_j T - \partial_j \partial_j T - Di(T + T_0) g_i v_i - \sum\nolimits_k \gamma_k \frac{Rb_k}{Ra} Di(T + T_0) \frac{\mathrm{d}\Gamma_k}{\mathrm{d}t} = \frac{Di}{Ra} \Phi. \tag{3}$$

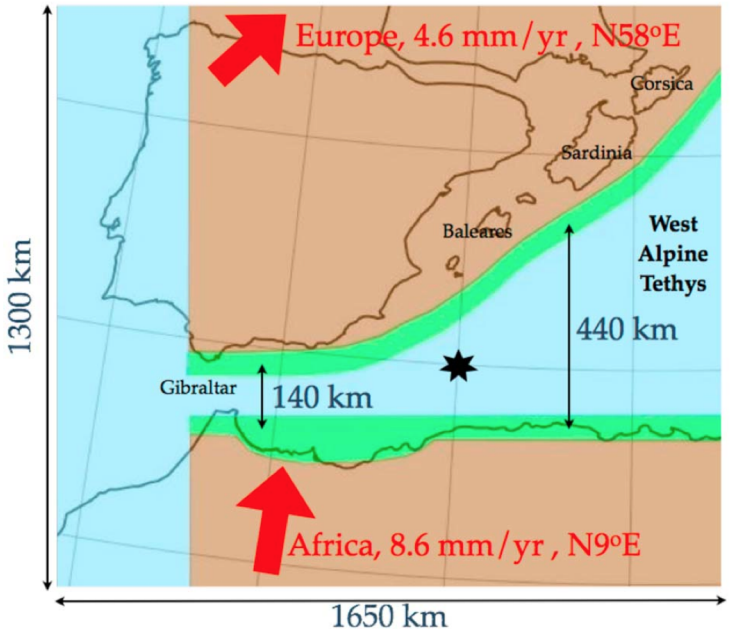

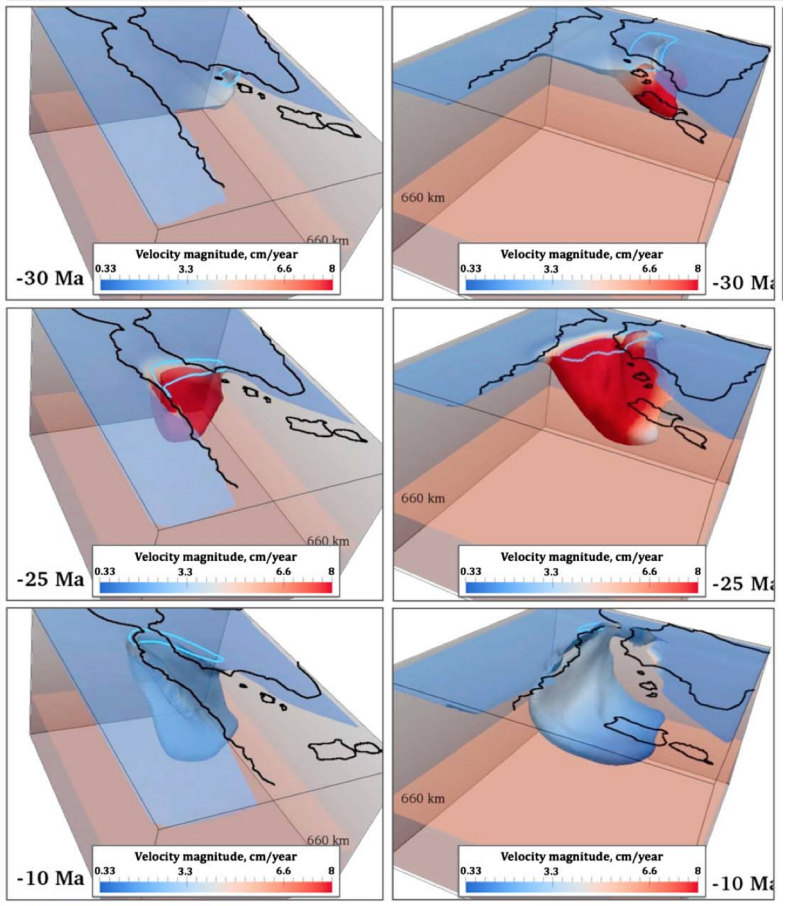

Figure 4. The top view of the modeled region showing the paleogeography at ~35 Ma [after *van Hinsbergen et al.*, 2014]. Brown regions are modeled as continental lithosphere, blue regions as oceanic lithosphere, and green regions denote continental margins. Location of active or incipient subduction at ~35 Ma will be indicated in Figure 6. The arrows denote the average absolute plate motion of Iberia and Africa over the past 35 Ma determined from *Doubrovine et al.* [2012]. From the reconstruction of *van Hinsbergen et al.* [2014] we estimate about 140 km of oceanic or transitional lithosphere between Iberia and Africa, and about 440 km between African and the Balearic margin. The average width of continental margins is 70 km. The star shows the position of vertical viscosity profiles in Figure 6.

Geochemistry Geophysics Geosystems G3
AN ELECTRONIC JOURNAL OF THE EARTH SCIENCES
Published by AGU and the Geochemical Society

Article
Volume 9, Number 4
12 April 2008
Q04019, doi:10.1029/2007GC001839
ISSN: 1525-2027

Click Here for Full Article

Formation and exhumation of ultra-high-pressure rocks during continental collision: Role of detachment in the subduction channel

Clare J. Warren
Department of Earth Sciences, Dalhousie University, Halifax, Nova Scotia, Canada B3H 4J1 (clare.warren@dal.ca)

Christopher Beaumont
Department of Oceanography, Dalhousie University, Halifax, Nova Scotia, Canada B3H 4J1

Rebecca A. Jamieson
Department of Earth Sciences, Dalhousie University, Halifax, Nova Scotia, Canada B3H 4J1

[1] UHP rocks commonly form and exhume during the transition from oceanic subduction to continental collision. Their exhumation in subduction channels depends on the balance between down-channel shear traction and up-channel buoyancy. Thermal-mechanical upper-mantle-scale numerical models are used to investigate how variations in material properties of the subducting continental margin affect this balance. Changes in shear traction leading to crustal decoupling/detachment are investigated by varying the onset of strain weakening, thermal parameters, and convergence velocity. Variations in buoyancy force are investigated by modifying subducted material density and volume. The model results are interpreted in terms of the exhumation number *E*, which expresses the role of the pressure gradient, channel thickness, effective viscosity, and subduction velocity. Peak metamorphic conditions, exhumation velocity, and timing of exhumation are temporally and spatially variable and are sensitive to the evolution of *E*. The models reproduce natural *PTt* constraints and indicate that neither slab breakoff nor surface erosion is required for UHP exhumation.

Components: 13,918 words, 11 figures, 4 tables, 5 animations.

Keywords: UHP metamorphism; exhumation; continental collision; subduction channel; crustal detachment.

Index Terms: 3613 Mineralogy and Petrology: Subduction zone processes (1031, 3060, 8170, 8413); 3654 Mineralogy and Petrology: Ultra-high pressure metamorphism; 8104 Tectonophysics: Continental margins: convergent.

Received 29 September 2007; **Revised** 21 December 2007; **Accepted** 10 January 2008; **Published** 12 April 2008.

Warren, C. J., C. Beaumont, and R. A. Jamieson (2008), Formation and exhumation of ultra-high-pressure rocks during continental collision: Role of detachment in the subduction channel, *Geochem. Geophys. Geosyst.*, *9*, Q04019, doi:10.1029/2007GC001839.

1. Introduction

[2] Crustal rocks metamorphosed to ultra-high-pressure (UHP) conditions have been described from many Phanerozoic continental collision zones. Their presence attests to burial of continental and (rarely) oceanic crustal material to, and subsequent exhumation from, depths of at least 100 km. Geochronological data from recent collision zones indicate that high-pressure metamorphism took place

$$\frac{\partial \sigma_{ij}}{\partial x_i} - \frac{\partial P}{\partial x_j} + \rho g = 0 \quad i,j = 1,2, \tag{1}$$

$$\frac{\partial v_i}{\partial x_i} = 0 \quad i = 1,2, \tag{2}$$

$$\rho c_p \left(\frac{\partial T}{\partial t} + v_i \frac{\partial T}{\partial x_i} \right) = K \frac{\partial}{\partial x_i} \frac{\partial T}{\partial x_i} + A + v_2 \alpha g T \rho, \tag{3}$$

where σ_{ij} is the stress tensor, x_i are the spatial coordinates, P is pressure, ρ is density, g is the gravitational acceleration, v_i are the components of velocity, c_p is specific heat, T is temperature, t is time, K is thermal conductivity, A is radioactive heat production per unit volume, and α is the volumetric thermal expansion coefficient. The last term in the heat balance equation is the temperature correction for adiabatic heating when material moves vertically at velocity v_2. For model T(+SH) (section 4), equation (3) also includes the effect of strain heating, $\sigma_{ij}\ \partial v_i/\partial x_j$, assuming that all dissipated mechanical energy is converted to heat.

2.5. Density Changes Associated With Metamorphic Phase Changes

[22] Nominal initial densities of crust and mantle materials (Table 1a) are for reference temperatures close to the average initial temperatures for each of these layers and represent thermally stable average continental and oceanic lithosphere. In all experiments, crustal materials undergo changes in density at pressure and temperature conditions corresponding to metamorphic phase changes. Densities and the metamorphic conditions at which they change are estimated from published data [*Hacker*, 1996; *Walsh and Hacker*, 2004], with maximum densities representing complete transformation to eclogite-facies phases. The densities of lower continental and oceanic crust (Table 1a) change across the eclogite field boundary; the higher density of ocean-crust eclogite reflects its mafic composition, whereas the intermediate lower continental crust has a lower eclogite-facies density. The density of quartz-bearing upper/mid continental crust increases across both the eclogite and coesite-eclogite facies boundaries (Table 1a). We test the sensitivity of exhumation mechanism and rate to changes in density of the subducted upper/mid-continental crust (Table 2).

[23] For materials that change density during a phase change we modify the incompressibility equation (2) to mass conservation, $\partial\rho/\partial t = -\partial(\rho v_i)/\partial x_i$ to account for the associated volume change and its effect on the buoyancy and velocity field. The volume change is calculated numerically as a modification to the implementation of incompressibility by applying additional normal, pressure/dilatational forces to finite elements at the time they are subject to phase-related density changes. The value of the excess pressure $\Delta P = \Delta\rho/\beta_v\rho$, where β_v is the viscous bulk modulus of the nearly incompressible material, and $\Delta\rho/\rho$ is the fractional change in density corresponding to the phase change. The excess pressure compresses material locally and only during the model time steps when the phase changes occur, thereby ensuring mass conservation. The fractional volume change accompanying a phase change is small in these models and its effect on the velocity field is

Rayleigh-Bénard convection

- Rayleigh-Bénard convection is a type of natural convection, occurring in a plane horizontal layer of fluid heated from below, in which the fluid develops a regular pattern of convection cells known as Bénard cells.

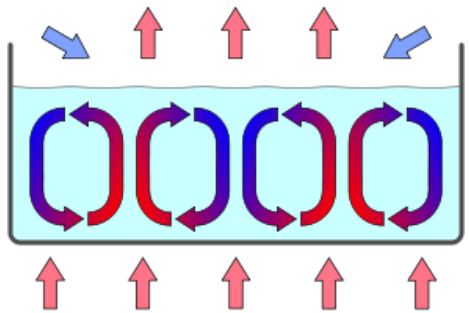

- Rayleigh-Bénard convection is one of the most commonly studied convection phenomena because of its analytical and experimental accessibility. The convection patterns are the most carefully examined example of self-organizing nonlinear systems.
- Buoyancy, and hence gravity, is responsible for the appearance of convection cells. The initial movement is the upwelling of lesser density fluid from the heated bottom layer. This upwelling spontaneously organizes into a regular pattern of cells.

Rayleigh number

In geophysics, the Rayleigh number is of fundamental importance: it indicates the presence and strength of convection within a fluid body such as the Earth's mantle. The mantle is a solid that behaves as a fluid over geological time scales.

When the Rayleigh number is below the critical value for that fluid, heat transfer is primarily in the form of **conduction**; when it exceeds the critical value, heat transfer is primarily in the form of **convection**.

A simple example of convection

Setup:

- I use my code ELEFANT
- box 4x3x1
- T=1 at the bottom, T=0 at the top
- free slip on all faces
- one incompressible material (BA)
- driven by buyoancy forces: $\rho = \rho_0(1 - \alpha(T - T_0))$
- $k = 1$, $\alpha = 10^{-5}$, $T_0 = 0$, $\mu_0 = 1$, $c_p = 1$, $\rho_0 = 1$

Initial temperature perturbation:

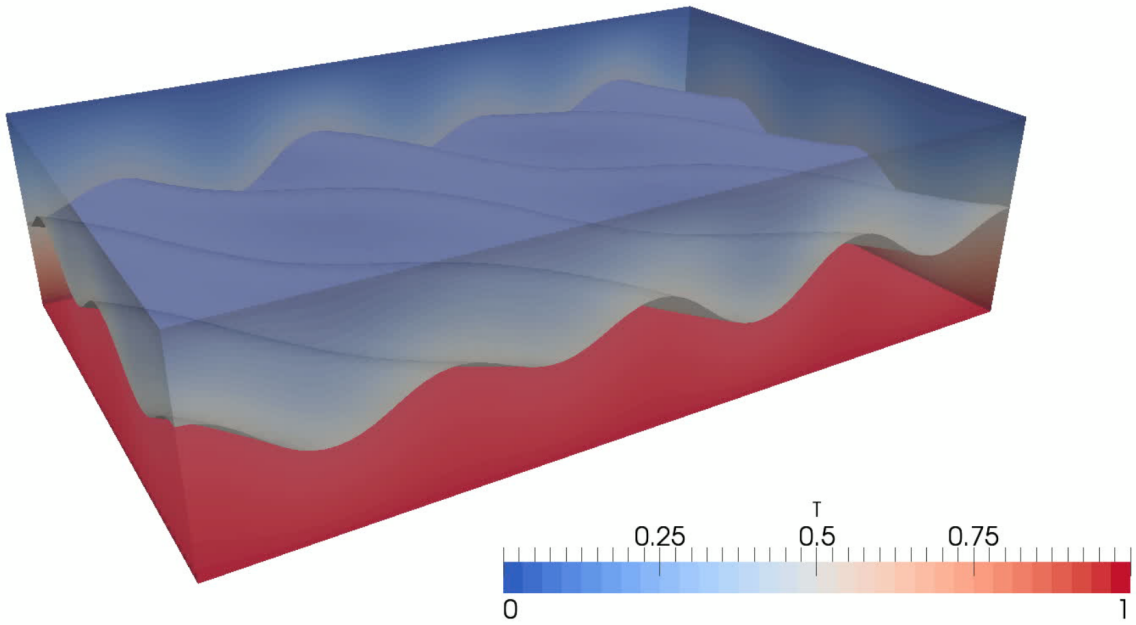

Since

$$Ra = \frac{\alpha_0 \rho_0 \Delta T g_0 h^3}{\mu_0 \kappa_0}$$

then

$$Ra = 10^{-5} g_0$$

I can choose Ra and it fixes my gravity vector magnitude g_0

Sub-critical Rayleigh number case: $Ra < Ra_c$

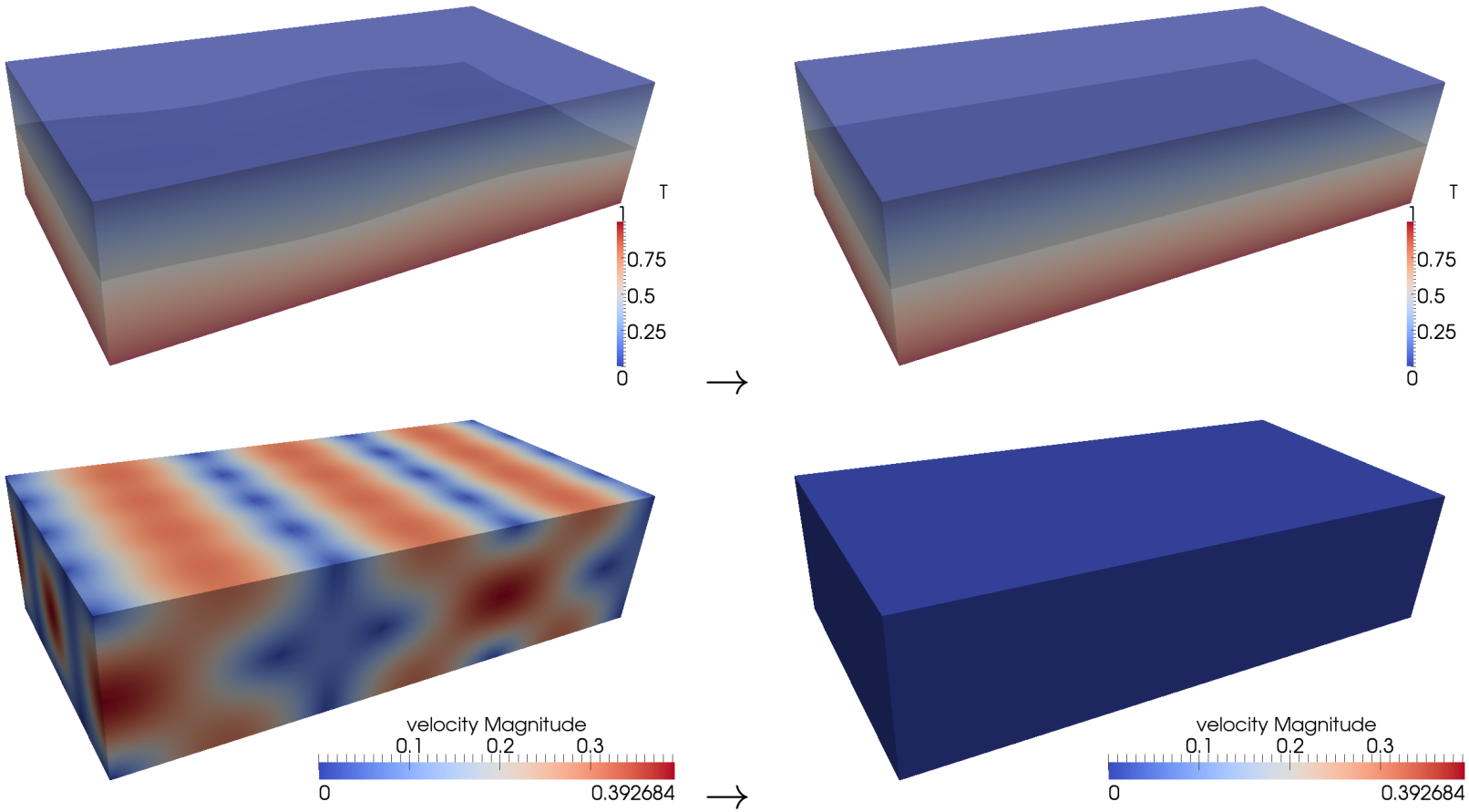

Initial temperature perturbation relaxes $\rightarrow$ 'pure' conduction.

Above-critical Rayleigh number case: $Ra > Ra_c$

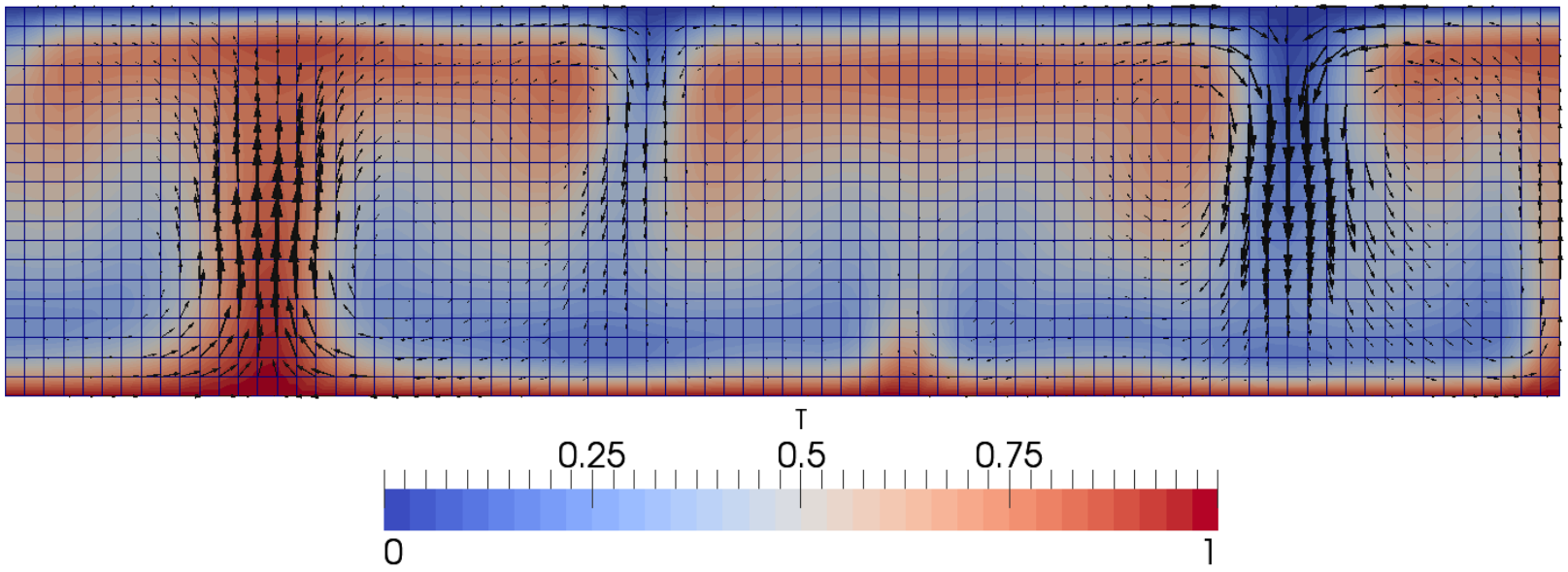

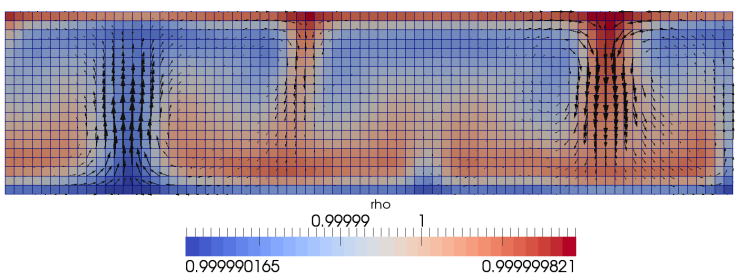

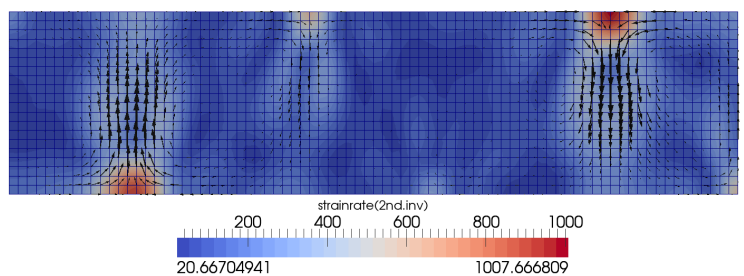

Cylindrical benchmark

A community benchmark for compressible mantle convection in a two–dimensional cylindrical domain

D. R. Davies, S. C. Kramer, C. R. Wilson, N. Tosi, J. Besserer, C. Hüttig

Early numerical models of mantle convection were commonly confined to two– and three–dimensional Cartesian domains, of limited extent. The actual geometry of mantle convection, however, is a three–dimensional spherical shell, with concentric spherical upper and lower boundaries. With improvements in numerical methods and increasing computational resources, global three–dimensional spherical mantle convection models are becoming more common (e.g. Baumgardner, 1985; Bercovici et al., 1989; Tackley et al., 1993; Bunge et al., 1996, 1997; Zhong et al., 2000; McNamara and Zhong, 2005; Tackley, 2008; Zhong et al., 2008; Nakagawa and Tackley, 2008; Davies and Davies, 2009; Schuberth et al., 2009; Wolstencroft et al., 2009; Stadler et al., 2010; Tan et al., 2011; Kronbichler et al., 2012; Burstedde et al., 2013; Davies et al., 2013). However, the use of this geometry for calculations at a realistic convective vigour remains expensive. As a consequence, simplifying geometries are often used, including the axisymmetric spherical shell (e.g. Solheim and Peltier, 1994; van Keken and Yuen, 1995) and the two–dimensional cylinder (e.g. Jarvis, 1993; van Keken and Ballentine, 1998, 1999; van Keken, 2001; Nakagawa and Tackley, 2005). Whilst there has been extensive benchmarking of Cartesian codes, for incompressible (Blankenbach et al., 1989; Travis et al., 1990; Busse et al., 1994; van Keken et al., 1997, 2008) and compressible (King et al., 2010) convection, in both two– and three–dimensions, there has been no benchmark in two–dimensional cylindrical geometry, which is our goal. As with previous community benchmarks, we focus on a comparison between derived quantities of the temperature and velocity fields from a number of carefully designed test cases, including the Nusselt number (Nu) and root–mean–square (RMS) velocity (V_{RMS}). Both incompressible and compressible convection are examined, following a structure very similar to that of King et al. (2010). The computational efficiency of each code is not compared, given the differing computational architectures available to each group.

The outline of this document is as follows: in Section 1, we present the equations and different approximations governing mantle convection. Benchmark cases are presented in Section 2, alongside the diagnostics used for comparing codes. Participants are asked to report all diagnostics, where possible. Codes contributing towards this benchmark are described in Section 3 (please provide a brief description if your code is not currently listed), with preliminary results from three codes: (i) Fluidity (Davies et al., 2011; Kramer et al., 2012); (ii) TerraFERMA (Wilson et al., 2013); (iii) Gaia (Hüttig et al., 2013); and (iv) Cheops (Besserer et al., 2011; Besserer, 2012); presented online at: `https://docs.google.com/spreadsheet/ccc?key=0AruSwf4D-LtMdHFjUHNscWFpR1FWcExyejkzM0lfTUE&usp=sharing#gid=0`. Access to this document will be granted, as requested. A discussion of results will be undertaken when all contributing codes have submitted final diagnostic values.

Setup

- I use my new code ELEFANTs
- 2D cylinder, $R_{in} = 1.22$, $R_{out} = 2.22$
- T=1 at the bottom, T=0 at the top
- free slip everywhere
- one incompressible material (BA)
- driven by buoyancy forces: $\rho = \rho_0(1 - \alpha(T - T_0))$
- $k = 1$, $\alpha = 10^{-5}$, $T_0 = 0$, $\mu_0 = 1$, $c_p = 1$, $\rho_0 = 1$

Initial temperature perturbation:

$$T(r,\theta) = R_{out} - r + 0.1\cos(4\theta)\sin((r-1.22)\pi)$$

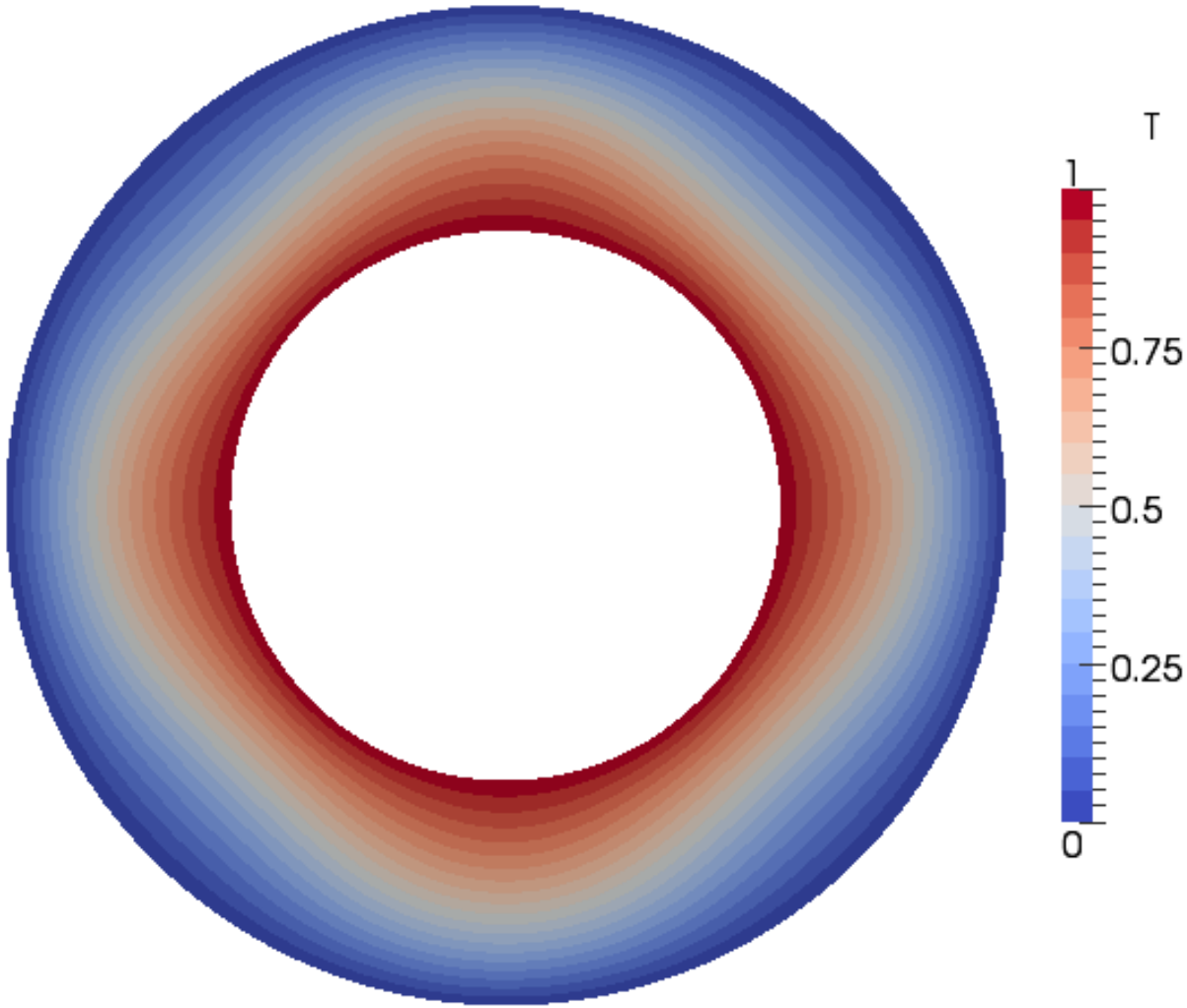

$Ra = 10^2$

$Ra = 10^4$

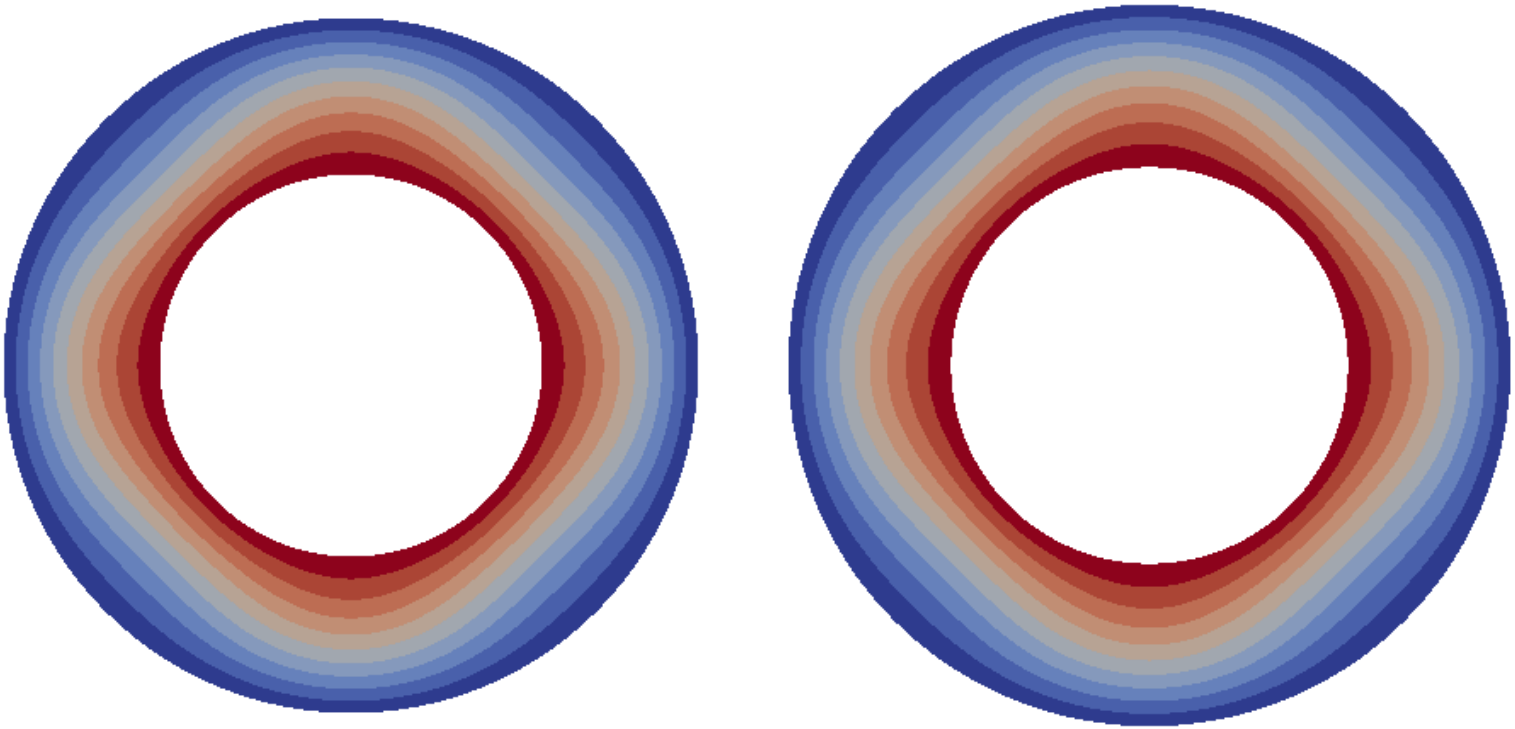

$t = 0.000$

$Ra = 10^2$

$Ra = 10^4$

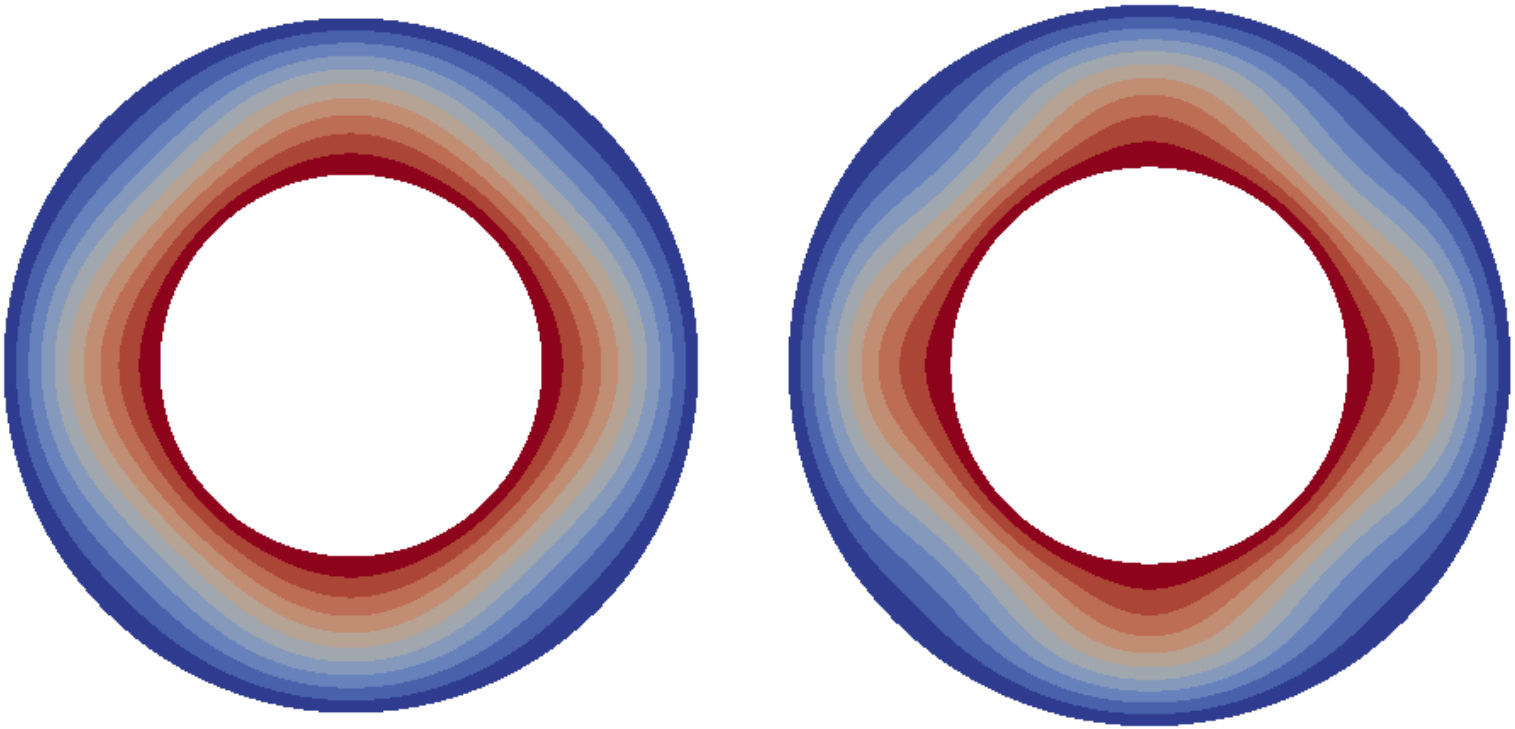

$t = 0.010$

$Ra = 10^2$

$Ra = 10^4$

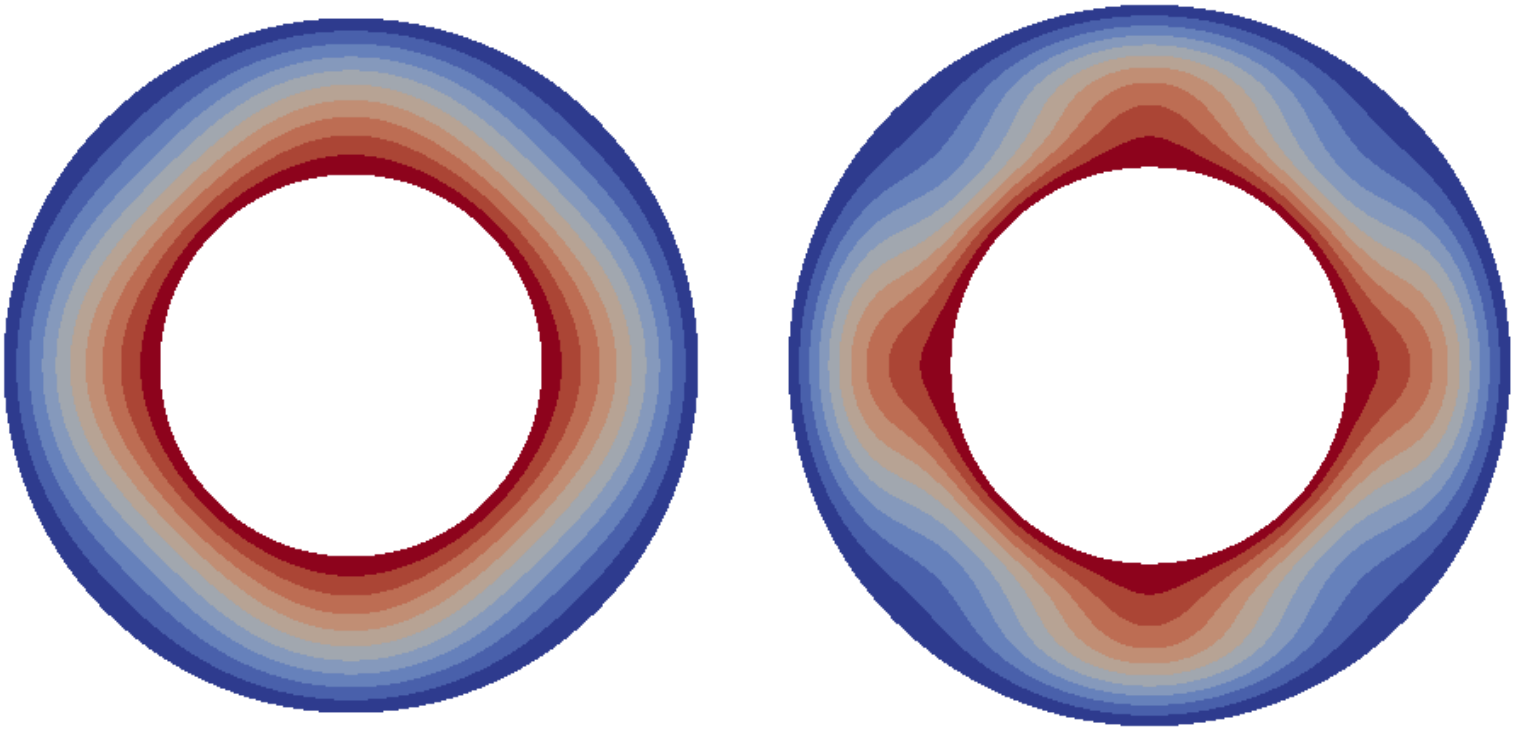

$t = 0.015$

$Ra = 10^2$

$Ra = 10^4$

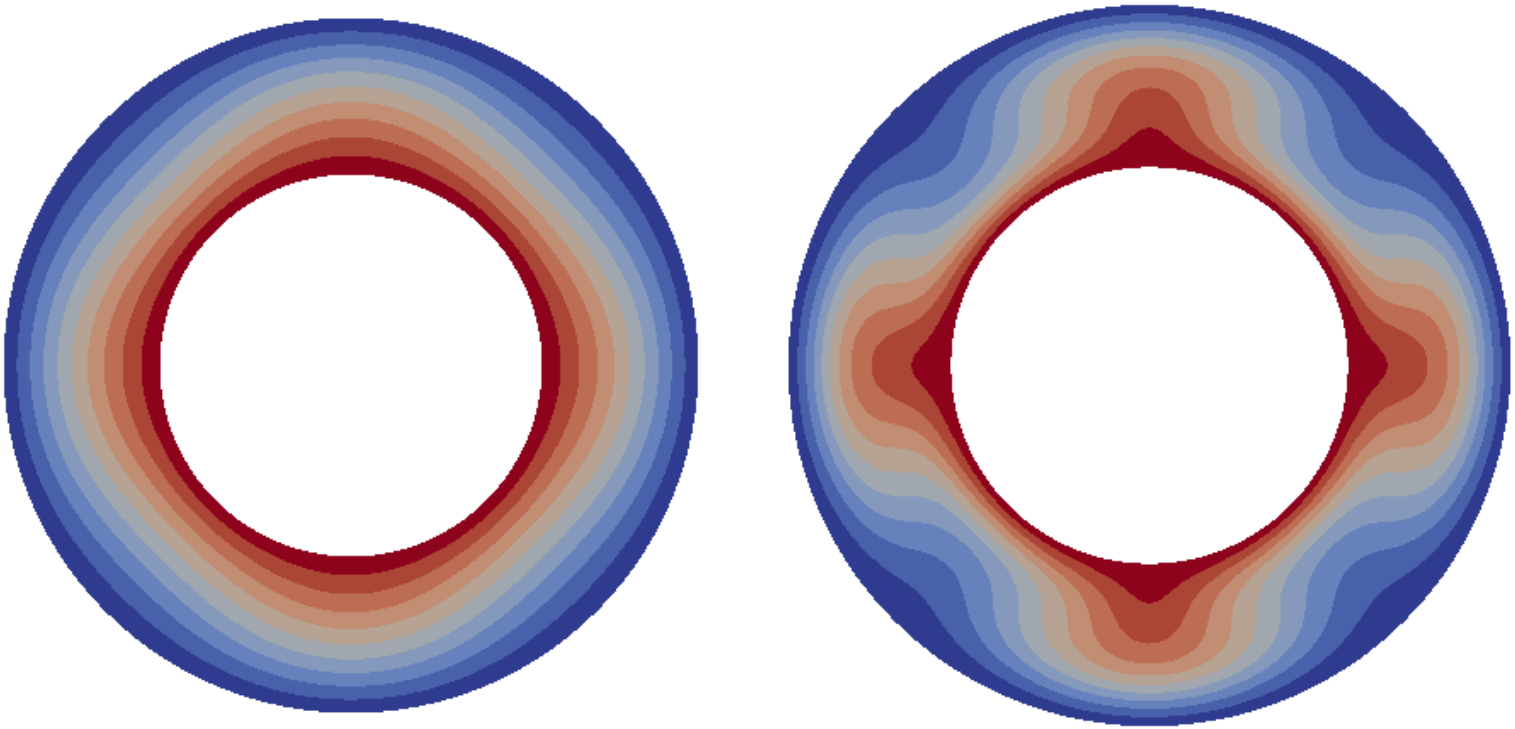

$t = 0.020$

$Ra = 10^2$

$Ra = 10^4$

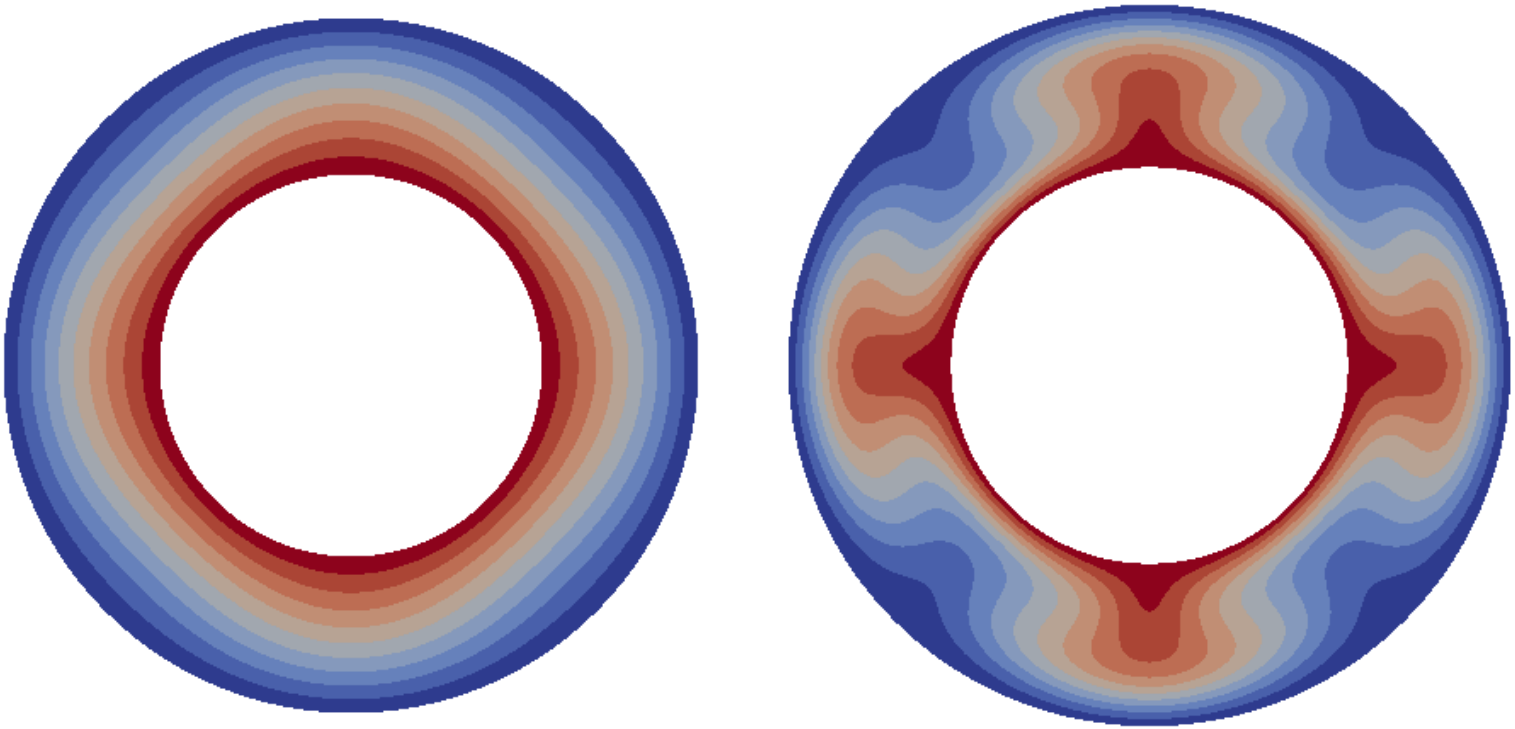

$t = 0.025$

$Ra = 10^4$ @ $t = 0.025$

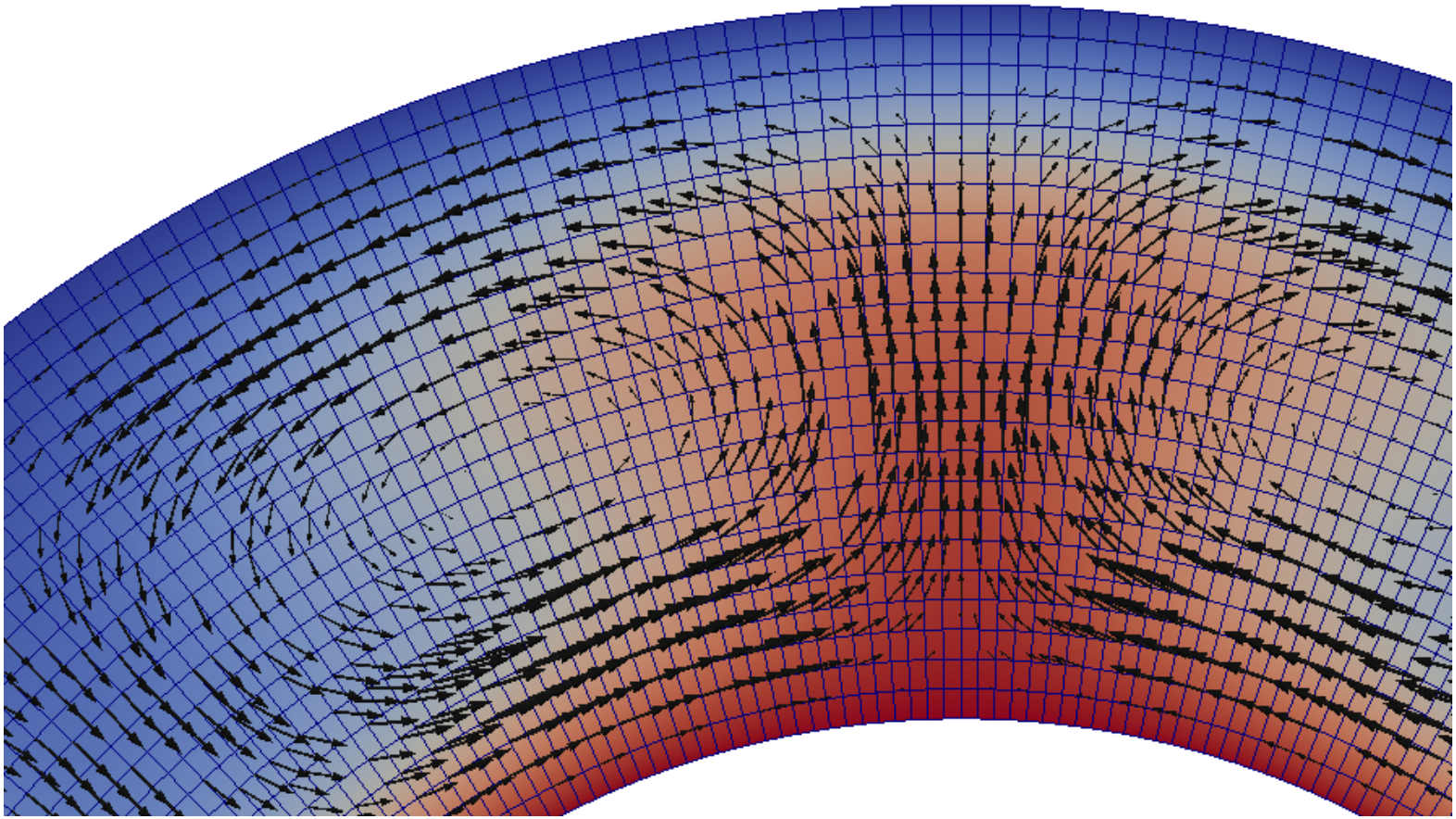

$Ra = 10^2$

$Ra = 10^4$

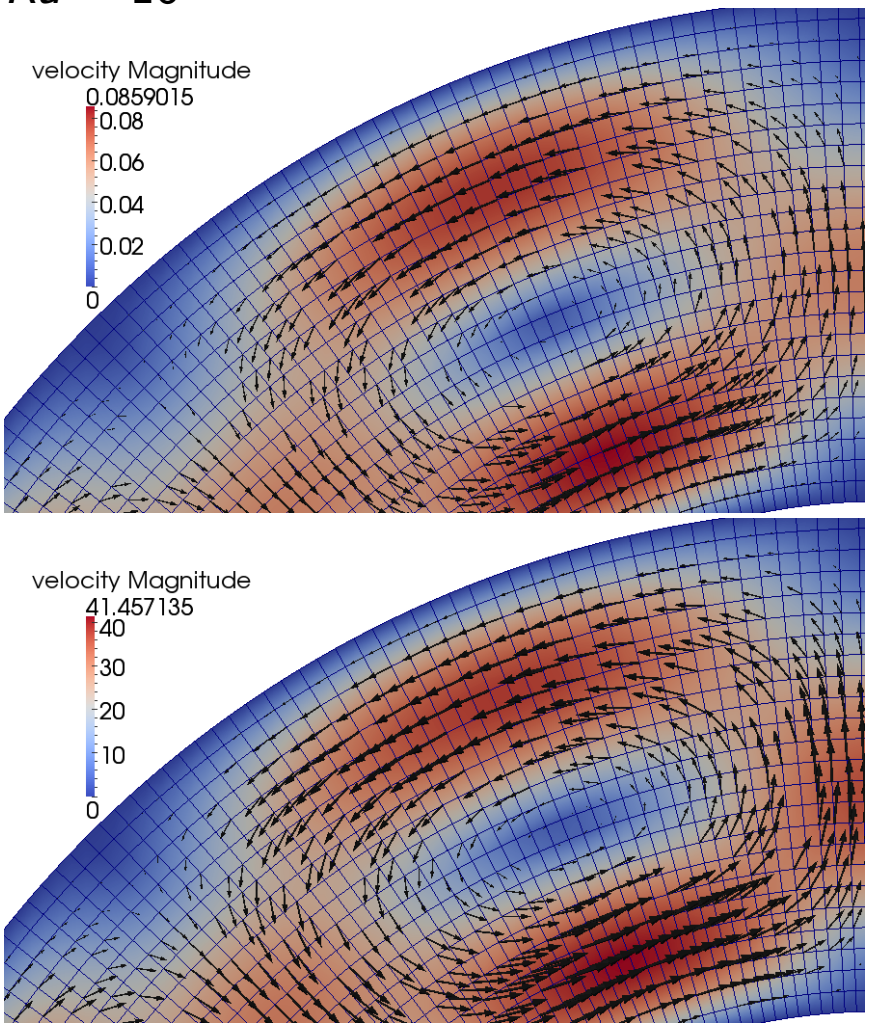

$t = 0.025$

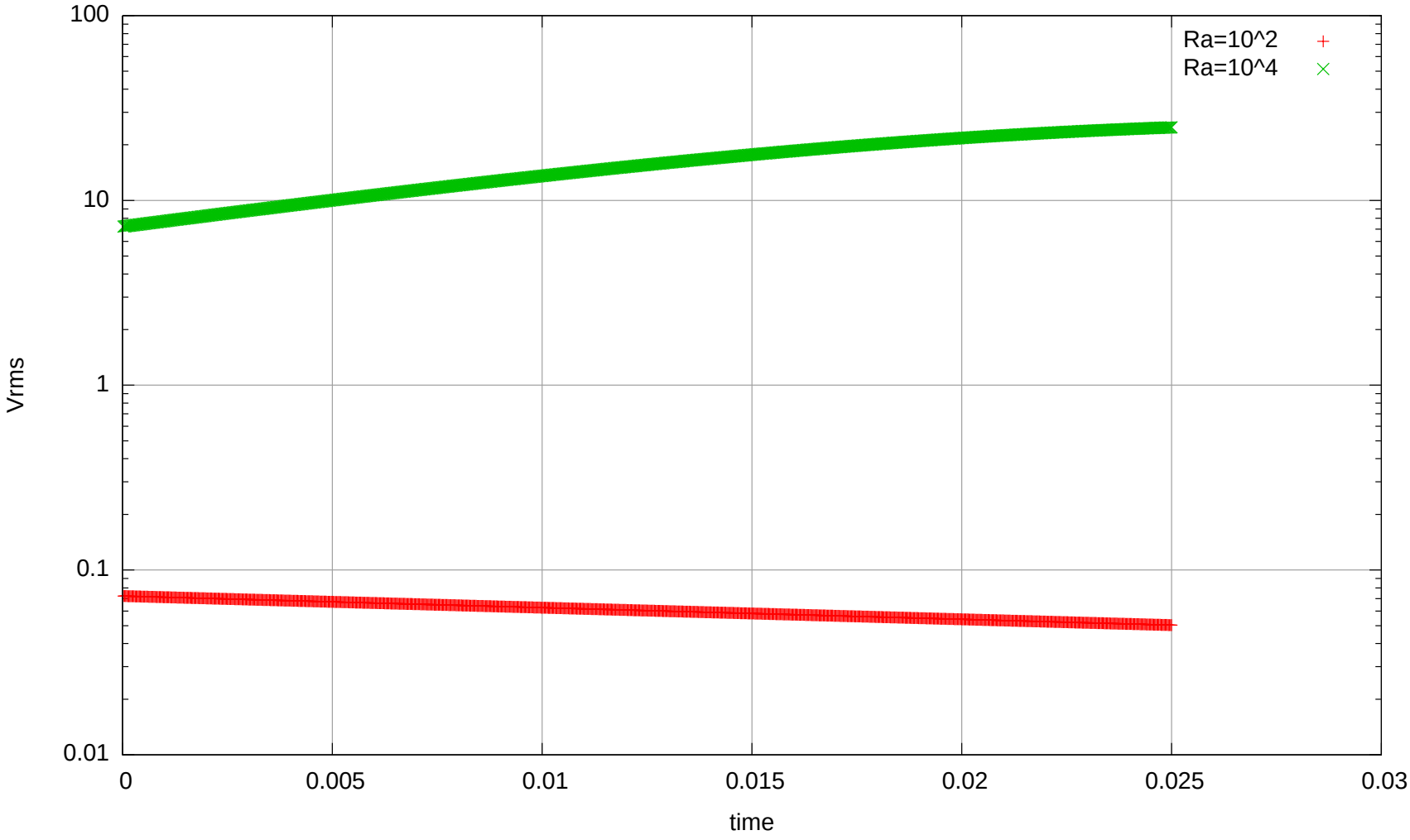
Ra=10^2
Ra=10^4
100
10
1
0.1
0.01
Vrms
0
0.005
0.01
0.015
0.02
0.025
0.03
time